An Experimental and Quantitative Analysis of *E. coli* Stress Response: Metabolic and Antibiotic Stressors

by

Inderpreet Singh Jalli

Department of Biology
Duke University

Date:_____

Approved:

_____
Frederik Nijhout, Supervisor

_____
Michael Reed

_____
Paul Magwene

_____
Kathleen Pryer

_____
Vikas Bhandawat

Dissertation submitted in partial fulfillment of
the requirements for the degree of Doctor
of Philosophy in the Department of
Biology in the Graduate School
of Duke University

2014

ABSTRACT

An Experimental and Quantitative Analysis of *E. coli* Stress Response: Metabolic and Antibiotic Stressors

by

Inderpreet Singh Jalli

Department of Biology
Duke University

Date:_____

Approved:

_____
Fred Nijhout, Supervisor

_____
Michael Reed

_____
Paul Magwene

_____
Kathleen Pryer

_____
Vikas Bhandawat

An abstract of a dissertation submitted in partial fulfillment of the requirements for the degree of Doctor of Philosophy in the Department of Biology in the Graduate School of Duke University

2014

Abstract

A series of experiments and mathematical models explore the behavior of the bacteria *E. coli* to stressors. Experimentally, the effect of L-homocysteine, a non-protein amino acid, is explored, and via math models, the effect of trimethoprim, a common antibiotic, is also explored. Previous work on L-homocysteine labels it a stressor, and this assertion is refined via the presented work. A mathematical model that improves on a previous work published by Kwon et al. (2008) explores the response of *E. coli* to various supplementations of amino acids when exposed to trimethoprim. A new approach towards disruption of the *E. coli* folate pathway and therapeutic drug treatments are also explored.

Dedication

"The first one to mix blue and yellow called the new color green," he said. "I want to do something similar to that."

"Excellent project," she replied, "it will look very good on your resume."

Contents

List of Tables

List of Figures

Acknowledgements

To my committee: Josh Socolar and Steve Haase for questioning the reasons why I was thinking about anything, Greg Wray for reasoning that I should not limit my thinking on anything, Mike Reed for reasonably questioning whether anything I was thinking about could be done by anyone, and Fred Nijhout for letting me think about and do anything… within reason.

To friends, family, and everyone I met while here, I wish every one of you the most happiness… may your lives be rivers of joy that nourish those around you.

1. Introduction

1.1 Folates and Trimethoprim

The folate cycle is critical to cellular reproduction and therefore is a common target for therapeutic agents, both for cancer treatment and antibiotic development. Trimethoprim, an antifolate antibiotic that directly targets the *E. coli* enzyme dihydrofolate reductase (DHFR), has been shown disrupt the function of the folate network by initiating a two-step domino effect [1]. First, trimethoprim inhibits DHFR and causes a spike in dihydrofolate (DHF_1). DHF_1 then inhibits the activity of folypolyglutamate synthetase (FPGS). The inhibition of FPGS disrupts the balance of polyglutamated folates in the *E. coli* cell. The level of polyglutamation is important, due to the specificity of enzymes to specific polyglutamated forms of folates such as tetrahydrofolate (THF). For example, methionine synthase E only utilizes THF_2 and higher glutamations for the conversion of L-homocysteine to L-methioinine [2]. In growth media without vitamin B12, *E. coli* expresses the methionine synthase H apoenzyme, but the enzyme is not catalytically active [3]. Kwon et al. discovered the inhibition of FPGS by DHF and developed a mathematical model of the domino effect that was fitted to time-course folate concentration data gathered under trimethoprim stress [1, 4]. Here we present a model of a broader set of folate responses to trimethoprim and metabolite supplements such as methionine and thymine. We also

present a mathematical model of increased DHF production, and we use this model to study mechanisms other than trimethoprim that can inhibit FPGS activity.

1.1.1 Folates:

Folates are a class of biological molecules that participate in the transfer of one carbon units in the biosynthesis of a broad diversity of metabolites. These metabolites include methionine, purines, and the universal methyl donor S-adenosyl methionine (SAM), which participates in some 150 different methyl transfer reactions. Biosynthesis of folate is by the combination of GTP and para-aminobenzoic acid. Once formed, folate can be polyglutamated to various degrees and enters the folate cycle as dihydrofolate (DHF). DHF is converted into tetrahydrofolate (THF) to form the core of the folate cycle [1]. Higher polyglutamated forms of THF have increased retention in cells, and some enzymes have higher preference or exclusive preference for certain polyglutamation levels of THF derivatives [5, 6]. Some enzymes however have no such preference. In *E. coli*, for example, one isoform of methionine synthase (MSH) accepts any polyglutamated form of 5-methyl-THF, while another exclusively functions on double glutamated 5-methyl-THF, and none lower [2, 7]. Polyglutamation of THF and its derivatives occurs via two enzymes, folylpolyglutamate alpha synthase and folylpolyglutamate gamma synthase (FP-α-GS, FP-γ-GS) [8, 9]. The second and third glutamations are gamma linkages, to the first and second glutamate respectively. Higher glutamations take the form of alpha linkages, added by FP- α-GS [8]. Kwon et al. found

that treatment of *E. coli* with trimethoprim causes a rapid increase in the DHF content of a cell, with a concomitant decrease in the activity of FP-γ-GS [4]. The spike in DHF also caused a subsequent increase in pABGlun and pteridines, of which DHF is a precursor [4]. Kwon et al. also found that only FP- γ-GS activity was inhibited by DHF [1]. Additionally, recent experiments have found that DHF is also a substrate of FP-γ-GS, further complicating the picture of the *E. coli* folate cycle (Andrew Bognar, personal communication).

1.1.2 Folate pathways across species:

While many organisms such as bacteria can synthesize their own folate, humans get folate from dietary sources [10]. In plants, chloroplasts are notable for a lack of folate enzyme expression despite the fact that the majority of methionine synthesis is carried out in chloroplasts [11, 12]. In *Rhodobacter sphaeroides* there is an unusual thymydylate synthase (ThyX) that can bypass DHF [13]. Enzymes across species also have differing responses to metabolite interactions. Kwon et al. reported the inhibition of *E. coli* FPGS by DHF, and no such inhibition has been seen in humans [1]. Human folate pathways employ a sarcosine dehydrogenase (EC 1.5.8.3), while *E. coli* shows no such activity [14]. While human interaction data with the methionine cycle and other metabolic pathways is well known, data on *E. coli* enzyme-metabolite interactions remain relatively sparse.

1.1.3 Antifolates and trimethoprim:

A major class of anti-cancer and antibacterial agents are the antifolates, which block function of the folate cycle in target organisms [15]. One common target for antifolates is dihydrofolate reductase (DHFR), which is inhibited by the antifolate trimethoprim [16]. DHFR converts the monoglutamated folate derivative dihydrofolate to monoglutamated tetrahydrofolate. THF is converted to 5-methyl-THF which donates a methyl group to homocysteine to form methionine. Methionine can also be formed by another route: homocysteine methyltransferase (HMT) transfers a methyl group from s-methylmethionine (SMM) and adds it to HCY [17]. SMM is not produced by *E. coli* however. This method is effectively a methionine cycle short-circuit, providing an organism the ability to create methyl groups without the use of 5-methylTHF, should SMM be available. However, this enzyme, while expressed in *E. coli*, has yet to be proven to be able to supplant folates as a methyl group source to make methionine [2, 17]. It is critical to maintain a proper balance of THF and its derivatives, lest a cell be deprived of one-carbon units that go towards DNA formation and protein methylation. Trimethoprim is a DHF analogue and is often used in conjunction with sulfamethoxazole. Sulfamethoxazole is an analogue of para-aminobenzoic acid (pABA) [10]. pABA, along with dihydropteroate diphosphate, is converted into dihydropteroic acid by dihydropteroate synthase (DHPS) [18]. Blocking production of DHF, and then the conversion of DHF into THF, is a far more effective strategy for antibiotic therapy

than using either drug alone, but resistance to this combination has increased in recent decades, some of it due to DHFR adaptations to trimethoprim [15, 19]. Trimethoprim binds to bacterial DHFR at 3000 times greater affinity than to vertebrate DHFR's [16]. Addition of trimethoprim can activate a stress response in *E. coli*, which causes upregulation of the stress protein UspA, and modulates expression of fur (ferric uptake regulation repressor), and lpdA (L protein component of the glycine cleavage enzyme system) [20]. Trimethoprim also induces expression changes in the SOS regulon, genes involved in pyrimidine synthesis, and genes in the mar regulon, responsible for antibiotic resistance [21].

1.1.4 Folate Enzyme List and Abbreviations:

Enzymes are listed with Uniprot ID and EC number. DHFR: dihydrofolate reductase (P0AFS3 / EC: 1.5.1.3), DHFS: dihydrofolate synthase (P08192 / EC: 6.3.2.12), TS: Thymidylate synthase (P0A884 / EC: 2.1.1.45), METH: methionine synthase (P13009 / EC: 2.1.1.13), METE: B12 independent methionine synthase (P25665 / EC: 2.1.1.14), FPGS: folypolyglutamate synthetase (P08192 / EC: 6.3.2.17), Pten: folate glutamate, pABA: para-aminobenzoate, pABn: para-aminobenzoylglutamate, DHF_n: dihydrofolate, DHP: dihydropteroic acid, THF_n: tetrahydrofolate, $5MTHF_n$: 5-methyl-THF, $5FTHF_n$: 5-formyl-THF, $10FTHF_n$: 10-formyl-THF, $510MTHF_n$: 5,10-methylene-THF, $510CH2THF_n$: 5,10-methenyl-THF, MET: L-methionine, SAM: S-adenosyl-L-methionine, SRH: S-ribosyl-L-

homocysteine, SAH: S-adenosyl-L-homocysteine, HCY: L-homocysteine, TM: trimethoprim.

1.2 Homocysteine

The bacterial stress response is critical to understanding the microbial responses to antibiotics [22-24]. L-Homocysteine (HCY), a toxic non-protein amino acid, has been widely interpreted as a stressor [25-28]. An elevated level of HCY is also implicated as a risk factor in cardiovascular disease and neurodegenerative disorders in humans [29]. Our presented work focuses on expanding the understanding of the response to HCY in Escherichia coli. We focus on growth of *E. coli* under exposure to HCY, and on the effect of HCY exposure on proteins in the methionine cycle that process HCY into methionine. We show that HCY does not universally depress the growth rate of *E. coli*, and that glucose supplementation in the growth medium can alter the response of methionine cycle proteins under HCY exposure.

1.2.1 Methionine Cycle Enzymes and Metabolites

The methionine cycle exists in all cellular organisms from plants to bacteria, and fungi to humans [30, 31]. The methionine cycle is linked to folate metabolism via methionine synthases which use methyl groups donated by folates to convert homocysteine to methionine. The methionine cycle contains S-adenosylmethionine (SAM), the universal methyl donor, and a host of methyltransferases that catalyze methylation reactions that play a role in epigenetics, biosynthesis and detoxification

reactions [32, 33]. SAM is also shunted into polyamine synthesis, which produces methylthioadenosine (MTA) [34, 35]. The structure of the methionine cycle is subtly different in taxonomically distant species. For instance, *E. coli* has two methionine synthases, vitamin B-12 independent and dependent (EC# 2.1.1.14 and 2.1.1.13), whereas *Arabidopsis thaliana*, *Saccharomyces cerevisiae* and humans have only one type that is B-12 dependent [7, 36]. Specific metabolites in the pathway also differ. *E. coli* produces S-ribosyl-homocysteine (SRH), while non-bacterial methionine cycles do not [37-39]. SRH is best known as the precursor of auto-inducer 2 (AI-2), a quorum-sensing molecule in bacteria [40]. *A. thaliana*, *S. cerevisiae*, *E. coli*, and human methionine cycles each feature variants of homocysteine methyltransferase (EC# 2.1.1.10, HMT) with different substrate affinities. *S. cerevisiae* express multiple HMT enzymes that cause short-circuits in the methionine cycle [39, 41-44]. The enzyme responsible for the *E. coli* short circuit has the same primary activity as the S. cerevisiae variant (SAM4), coupling the SAM -> SAH and HCY -> MET conversions. However the *E. coli* variant also assimilates S-methylmethionine (SMM), and in *S. cerevisiae*, SMM is catabolized by a different enzyme, MHT1 [45, 46]. *E. coli* also carries out a SAM to MET conversion without the use of HCY or SAH, via the enzyme ThiH (EC# 4.1.99.19) [47]. *H. sapiens* has two HMT variants, both able to catabolize SMM [17]. HMT enzymes in all studied species catabolize SMM, despite the fact that it is only known to be generated by angiosperms [17, 39, 44, 45]. This suggests that the HMT's have probably evolved to catabolize plant-

derived SMM. A. thaliana generates SMM via a methionine cycle short-circuiting enzyme, methionine methyltransferase (MMT, EC# 2.1.1.12) in A. thaliana, and is assumed to introduce stability in the A. thaliana methionine cycle, buffering it from spikes in methionine [38, 48, 49]. Figure 1 illustrates some of the differences between methionine cycles in major study species.

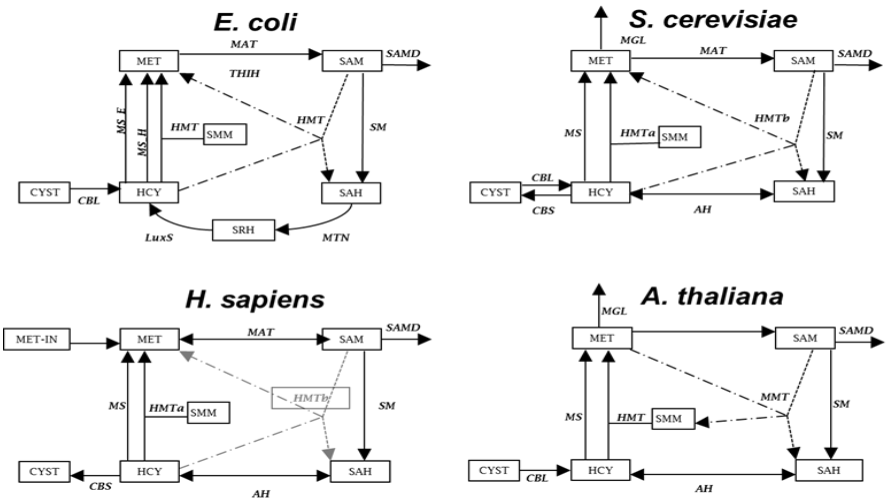

Figure 1: The methionine cycle across organisms

Variation in the Enzyme/Metabolite map of the MET CYCLE: Small differences in the metabolic map are presumably the result of adaptation to particular selective pressures and life histories. We see broad similarities in metabolites and enzymes, but subtle differences. In some organisms such as *S. cerevisiae*, control points differ greatly from others. HMT isozymes, selenium processing, and some inputs such as methionine from plasma or phloem are not shown to avoid complexity.

1.2.2 HCY stress biochemistry in microorganisms:

Exposure to acetate causes an increase of HCY in *E. coli* and strongly inhibits growth, along with a depletion of intracellular methionine [50]. Acetate-induced inhibition is ameliorated by addition of methionine to growth medium [50]. Increased levels of intracellular HCY lead to its conversion into homocysteine thiolactone (HCY-T) by methionyl tRNA synthetase, and secretion of HCY-T into the extracellular space, a process that also occurs in S. cerevisiae [51, 52]. When HCY is added to growth medium directly, isoleucine and to a lesser extent alanine ameliorate growth inhibition, but methionine does not [25]. Neither HCY-T nor the dimer, homocystine, have any effect when added directly to growth medium. Other microorganisms such as Salmonella enterica, and S. cerevisiae also experience growth inhibition when exposed to HCY at sufficient concentrations [25, 52]. The severity of growth inhibition is dependent on both HCY dosage and organism cell density in media [25]. There are exceptions, with some strains of wild-type or CBS deficient *S. cerevisiae* being relatively immune to an addition of HCY to growth medium [53].

1.2.3 MET cycle regulation in Enterobacteriaceae:

The methionine cycles of the enterobacteria *E. coli* and *Salmonella typhimurium* are similar, having the same enzymes, regulatory proteins, and metabolites, but with subtle kinetic differences [54]. The regulatory proteins, METJ and METR, and the enzymes METE and METH, are influenced by HCY exposure [34]. METE and METH enzymes

convert HCY to methionine. All methionine cycle genes, except METH, appear to be negatively regulated by METJ, which requires S-adenosyl methionine (SAM) as a co-repressor for maximum activity [55-59]. METJ also represses METL, and, META, METB, METC, METK, and METF [58-61]. METR positively regulates METE and METH, in addition to negatively autoregulating itself [54, 62-67]. HCY activates METE, and inhibits both METR and METH [56, 68-70]. Fraser et al. however have found that on exposure to HCY, METE mRNA is downregulated [26]. We expand on these prior studies of methionine cycle regulation, and establish explicit quantitative relationships between METJ, METR, METE and METH under a broad variety of nutrient conditions and under HCY stress.

1.2.4 Significance:

The response to HCY in microorganisms has been primarily studied at high toxic concentrations, which preclude a full understanding of its effects on physiology. In the present study we expose *E. coli* to a broad range of HCY concentrations and sample growth at high temporal resolution. We show that the response to HCY is nutrient-dependent and that under certain conditions HCY can enhance growth, and we correlate the growth response to variation in regulatory proteins and enzymes in the bacterial methionine cycle. By studying the response to HCY under a broad range of exposures and under different nutrient backgrounds we show that the stress response is conditional and that under some circumstances HCY can act as a nutrient and actually

enhance the growth of *E. coli*. Through high fidelity proteomics we also show an instance of Simpson's Paradox in the regulation of METR by METJ.

1.2.5 Homocysteine Abbreviations / definitions:

Uniprot numbers and EC numbers are given for enzymes where appropriate. HCY : L-homocysteine (all experiments in this study were conducted with L-HCY), MET : L-methionine, S-adenosyl-L-methionine : SAM, SAH : S-adenosyl-L-methionine, CYSTA : L-cystathionine, SRH : S-ribosyl-L-homocysteine, METH: B12 dependent methionine synthase (P13009 / EC: 2.1.1.13), METE: B12 independent methionine synthase (P25665 / EC: 2.1.1.14), METJ : Met regulon regulatory protein MetJ (P0A8U6), METR (P0A9F9), RPoS (P13445). "Defined media" – referring to any media comprised of exact chemical components (in this study, M9). "Rich media" – referring to any media comprised of loosely defined cell extracts and the like (in this study, LB).

2. Quantitative Considerations on Folates

2.1 Methods:

2.1.1 Folate Pathway Model Experimental Data:

Folate concentration data employed in this study were measured in the manner described in Kwon et al. 2008 [1, 4]. Folate concentrations were measured absolutely, and are referenced throughout this paper in μM units. Scenarios for folate measurement are: TM added to growth medium without supplementation, (No Supplement); TM added with previously supplemented minimal medium: Glycine, Inosine, Methionine (GIM); Glycine, Inosine, Methionine, and Thymine (GIMT); and Inosine only (I). All supplements were added at 0.3 mM in growth medium before media sterilization. *E. coli* strain NCM3722 was used for all folate measurements and is referred to in Kwon et al. and in this study as wildtype [1]. Unless otherwise stated, cells were grown in Gutnick minimal salts medium (Sigma-Aldrich), in a shaking flask at 37°C.

2.1.2 Simulations:

All simulations, parameter estimations, and calculations were carried out in Matlab version 2012b, on an Intel Q8200 2.33GHz processor, using Microsoft Windows 7, 64-bit, and ODE solver ode15s. Unless estimated via optimization, enzyme kinetic parameters were taken from previously published experiments. If no kinetic or reaction rate information was available from previous experiments, then the parameters were fitted via the Global Optimization Toolbox in Matlab. Certain enzymes were converted

into linear approximations and their rates were estimated. Simulations were carried out using the Simbiology Toolbox in Matlab. Metabolite concentrations were set as variables, with parameters being kinetic constants, input flux of mass into and out of the system (simulated with a linear equation unless otherwise stated), Vmax of enzyme kinetic equations, and cofactor concentrations.

2.1.3 Folate Pathway Model Equation Setup:

Folate metabolites are usually converted into different forms by enzymes. Each enzymatic conversion is represented by a different equation. Some conversions are non-enzymatic. Enzymatic (non-linear) conversions of variables were modeled by the Michaelis Menten equation:

$$v = \frac{d[P]}{dt} = \frac{V_{max} * [S]}{K_m + [S]}$$

Equation 1: Simple Michaelis Menten Equation

Where Km is the Michaelis constant, [S] is the concentration of the substrate, and Vmax is the maximum rate achieved by the system [71]. For well-studied enzymes, more descriptive and accurate kinetic equations were available, for example, for FPGS, which had inhibition data from the folate DHF and employed competitive inhibition:

$$v = \frac{d[P]}{dt} = \frac{V_{max} * \frac{THF_1}{K_m}}{1 + \frac{DHF_1}{K_i} + \frac{DHF_1}{K_i} + \frac{THF_1}{K_m} + \frac{THF_2}{K_m}}$$

Equation 2: FPGS Equation

If a variant of the Michaelis Menten equation is not used, or a non-enzymatic conversion is modeled, a linear rate equation is employed instead with the following form:

$$v = [S] * k_s$$

Equation 3: Linear Equation

2.1.4 Folate Pathway Model Elements:

The structure of the *E. coli* folate pathway model is presented in Figure 2. Variables are the source/sink for folates, and the folates DHF_n and THF_n, at three glutamation levels (boxes). The mathematical model treats all previously mentioned forms of THF, for which considerable experimental data exists, as one of three summated variables that are only differentiated by glutamation level. THF glutamations are converted from THF_i to THF_{i+1} by the enzyme FPGS (ovals). In this model, only FP-γ-GS activity, which converts THF_1 to THF_2 and THF_2 to THF_3, is included. Vmax for both activities is FPGS_n1_Vmax (THF_1 to THF_2) and FPGS_n2_Vmax (THF_2 to THF_3). These

two Vmax values are independent to balance the summation of all THF analogues into one entity. DHF_n and THF_n are recycled back into the source via a linear rate constant. Conversion between DHF_n and THF_n is a linear rate equation. A critical feature of the model is DHF inhibition of FP-γ-GS. Kwon et al. found that DHF does not inhibit FP-α-GS, but that the spike of DHF caused by the inhibition of DHFR by TM is instrumental in explaining the dynamics of folate response to TM [1, 4]. The model replicates the spike of DHF set into motion by TM. The current model differs from the model of Kwon et al. in the following ways: first, in the Kwon model the DHFR reaction was allowed to continue in a lowered capacity in the presence of TM [1]. The current model disallows that possibility (see double lined dashed arrows from DHF_n to THF_n). In addition, the earlier model did not feature recycling from any folate derivatives, instead keeping sinks and sources constant and separate. Our model merged the sinks and sources, and treated the combined entity as a single variable.

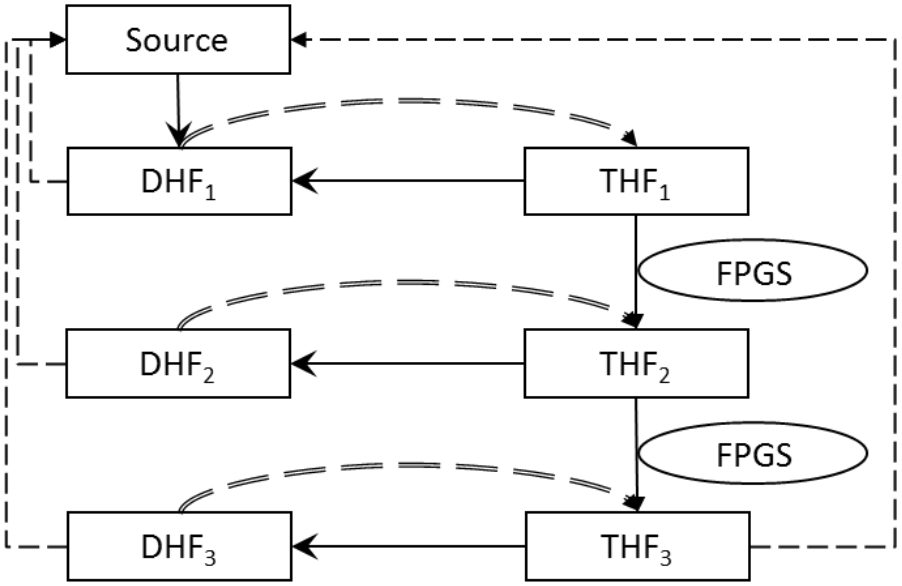

Figure 2: Kwon model and modifications in current model -

(Ovals = enzymes, boxes = metabolites or sources, solid lines = linear conversion rates, narrow dashed lines = recycling of folates added, thick dashed lines = DHF_n to THF_n conversion removed from Kwon model [1]. The current model differs from the original Kwon et al. model in a few key ways. The Kwon model allowed for some conversion of DHF_n to THF_n by DHFR in the presence of trimethoprim, and the current model does not [1]. The model also allows for recycling of folates into the source for DHF_1, because even under trimethoprim stress, folate recycling into Pte_n or pAB_n occurs.

2.1.5 Folate Pathway Model Parameter estimation:

The multiple growth conditions and experimental replicates under which time course folate concentration data were gathered allowed us to carry out a nested

parameter fit of kinetic constants, Vmax parameters, and linear conversion constants. Global parameters such as enzyme kinetic constants for substrates (Km) and inhibition constants (Ki) were held constant across all growth condition. Parameters which could potentially vary between growth conditions, such as input and output fluxes to the system, and Vmax parameters of enzymes, were designated as, "local," parameters, constant within each scenario. Parameters were estimated by sequential use of the genetic algorithm function, followed by a more sensitive parameter optimization which utilized the Matlab function fmincon. Once the genetic algorithm found a coarse solution that avoided getting trapped in local minima, the fmincon function refined the accuracy of the parameter search. Since the model treats all THF analogues as one, we created a global parameter search for the inhibition Ki of DHF on FPGS. In the previous study, the parameter was set to 3.1 μM. Since FPGS has a variety of individual THF targets, we fitted a Ki to the data instead using an experimentally derived constant. The fit of this parameter was carried out under stringent conditions.

2.1.6 Reaction acceleration model:

The traditional method for influencing physiological systems has been to inhibit a target enzyme to slow down the reaction it catalyzes. Enzyme targeting for the purposes of antibiotic development is centered on finding substrate-like molecules that will severely lower the activity of the target enzyme. Here we mathematically model another method: accelerating an enzymatic reaction to perturb bacterial physiology and

mimic the functioning of an established antibiotic, TM (Figure 3). While not as popular as enzyme inhibition, the proposal is not without precedent. In a simplified mathematical model of the *E. coli* folate system, we artificially speed up DHFS production of DHF, and allow it to overcome the ability of DHFR to break down DHF.

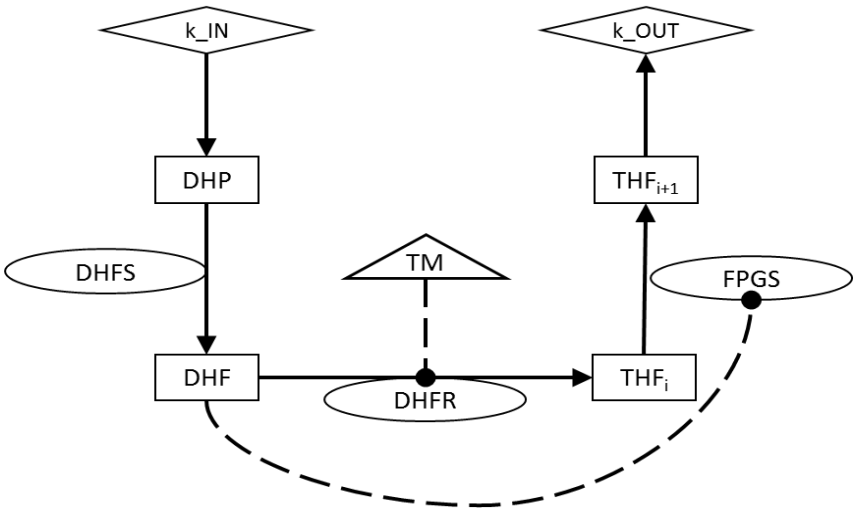

Figure 3: Reaction Acceleration Model

Ovals = Enzymes, Triangle = Trimethoprim, Rhombuses = input/output linear reactions, dashed lines = inhibition interactions. Trimethoprim (TM) inhibits DHFR, and dihydrofolate inhibits FPGS.

2.2 Folate Results:

2.2.1 Statistical analysis of folates with and without amino acid supplementation:

Trimethoprim is added into growth media of *E. coli* at O.D. ~0.5. At time zero, trimethoprim is not present in media, but once added its effect can be seen in Figure 4 (adapted from Kwon et al. 2008), where the balance of folate pools is changed

dramatically. DHF_1 and DHF_2 increase by approximately two orders of magnitude, and so do pAB_1 and pAB_2. DHF_3 and pAB_3 however show relatively little change. THF_1 and Pte_1 increase by about one order of magnitude, and as do THF_2 and Pte_2. THF_3 drops significantly, while Pte_3 increases.

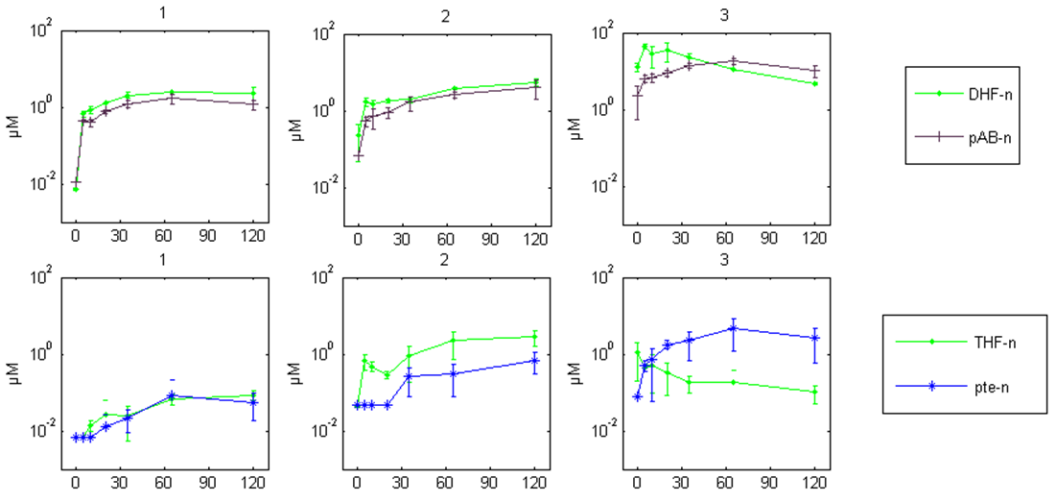

Figure 4: Folate disruption under trimethoprim, without supplementation: TM at 4 μg / mL in growth media caused a decrease in reduced folates and an increase in oxidized folates. After an initial decrease, reduced monoglutamates and diglutamates increased.

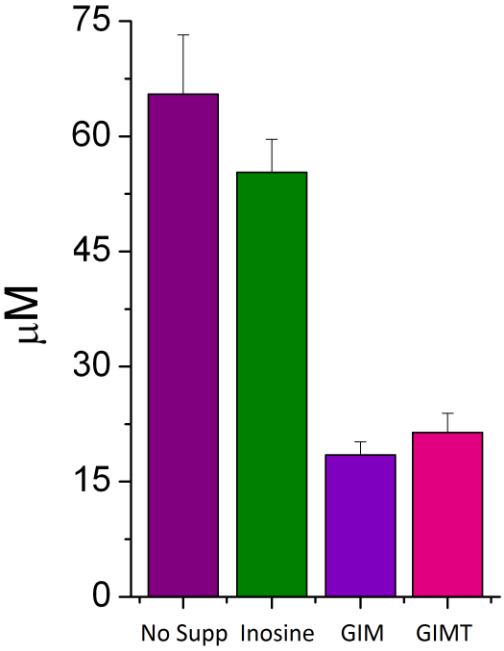

Figure 5: Total Cell folate concentrations under supplementation

When supplemented with amino acids, total folate concentrations in the cell decrease. Under Inosine supplementation, total folate concentration drop is trivial, but under multiple supplementations, folate drop is pronounced.

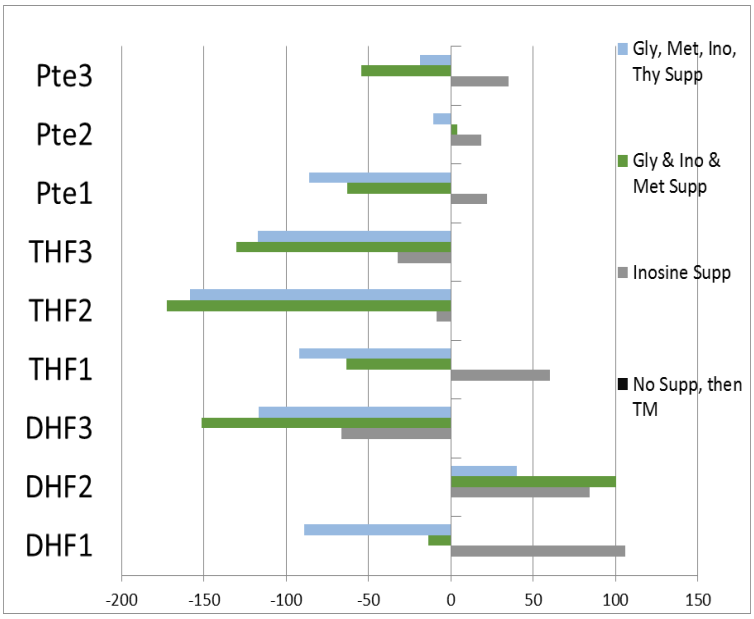

Figure 6: Individual Folates under Supplementation:

A percent difference calculation on folate concentration under various amino acid supplementations. Folates are sampled at time zero across supplementation scenarios. Almost all folates drop across all supplementation conditions, except for DHF_2, which shows no drop when compared to non-supplemented TM treatment. Pte_2 also shows increase in a variety of supplementation conditions.

2.2.2 Folate Pathway Model parameter estimation across supplementation conditions:

Parameter fitting yielded a global Ki for DHF on FPGS of 5 μM, different from the 3.1 μM gathered from assaying FPGS activity directly on THF_1 with DHF_1 [1]. This is an estimate of all DHF inhibition activity with respect to FPGS activity on both THF_1 and THF_2. Across the five simulation conditions, local parameters such as FPGS Vmax and input/output reaction rates differed widely (Figure 8). Percent differences of estimated local parameters were calculated relative to the No Supplementation condition. In all conditions, the rate of conversion of THF_2 to DHF_2 dropped with respect to the no supplementation condition. The Vmax of FPGSn1Vmax, which is the Vmax of conversion of THF_1 to THF_2 increased. DHF_1 recycling increased as well. Other parameters were more balanced in their change from the No Supplementation condition.

2.2.3 Folate Pathway Model simulation results across supplementation conditions:

The No Supplementation scenario simulation results are shown below along with experimental data (Figure 7), and further simulation results are shown in the supplementary. The simulations capture a general trend of a sharp increase of DHF_1 and DHF_2 during the 120 minute time course of the experiment.

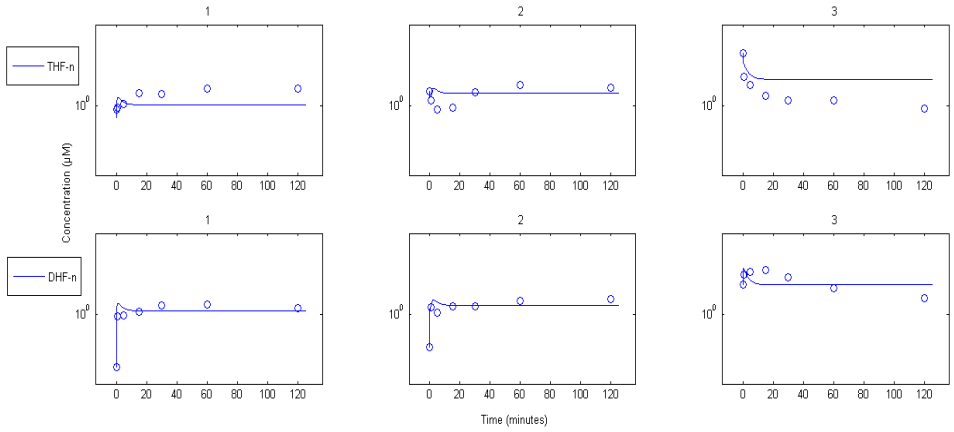

Figure 7: Simulation and experimental folate progression:

This behavior is partially captured by the mathematical model, and improves upon the previous model in accuracy with most metabolites.

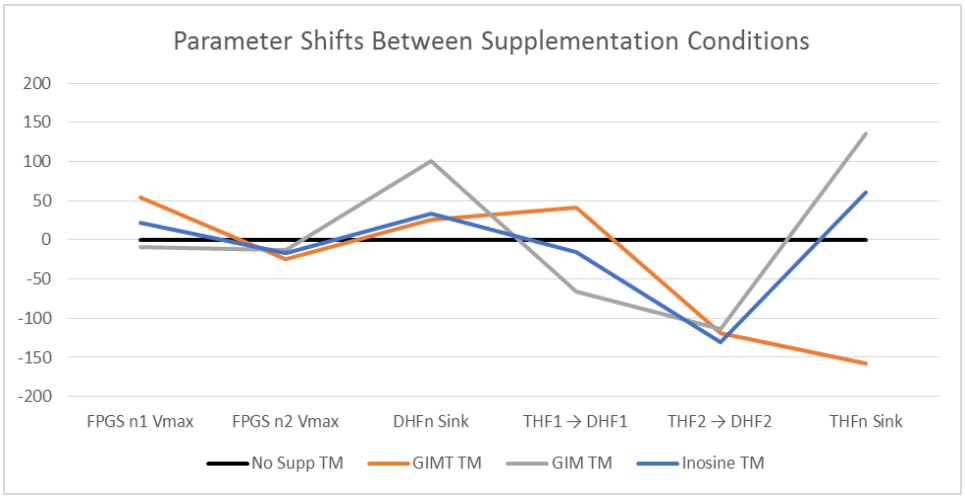

Figure 8: Percent difference of parameter estimates in supplementation conditions:

The no supplement condition is used as a baseline for assessing the parameter changes across various supplement conditions. All supplement conditions varied

nontrivially with respect to the original TM only condition, and FPGSn2Vmax changed the least of all parameters from the TM only condition.

2.2.4 Mathematical modeling of DHFS activation:

A simplified model of the folate network was created to test a hypothetical antibiotic treatment of *E. coli* wherein DHFS is accelerated. The aim of this model was to test whether an acceleration of the dihydrofolate synthase reaction, which creates DHF, could provide suppression of FPGS, which is a major driver of the *E. coli* response to TM. Recall that TM functions by suppressing the activity of DHFR, causing a spike in DHF, which then suppresses the activity of FPGS (Figure 3). The drop in polyglutamated THF analogues slows down other enzymes such as methionine synthase, which need polyglutamated THF to function. Figure 9A shows the control condition in solid lines, where concentrations of DHF, THF_i, THF_{i+1}, and DHP are reported. When TM is introduced into the system, the effect of is displayed with dashed lines, with a large spike in DHF, and a drop in THF_{i+1}. Figure 9B shows how a three order magnitude drop in the Km of DHFS causes a spike in DHF, and a corresponding spike in THF_i with respect to the control. The result is not as dramatic as the effect of TM.

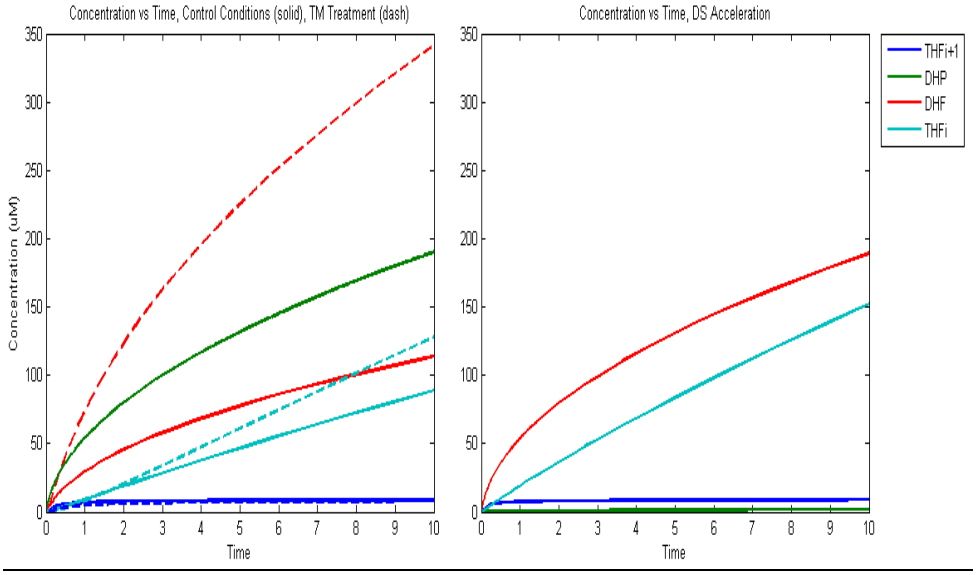

Figure 9: Modeling DHFS rate increase:

This simulated "enzyme acceleration" creates a spike of DHF_n which inhibits FPGS, and produces the same general disruption in the folate network as TM, albeit at a lower intensity. In this case, no disruption of DHFR is created, as with TM.

2.3 Folate Discussion:

2.3.1 Folate concentrations under amino acid supplementation:

Total concentrations of all folates drop in supplemented conditions with respect to the non-supplemented condition (Figure 5). Most individual folate concentrations decline under amino acid supplementation when compared to the non-supplemented condition (Figure 6). Folate conversion reactions are linked to amino acid metabolism. Methionine synthase (MS) uses 5MTHF to produce methionine from homocysteine, and

serine hydroxymethyltransferase (SHMT) reversibly interconverts serine and THF to produce glycine and 510MTHF [32, 72, 73]. THF, the precursor to 5MTHF and 510MTHF, is produced via an NADPH consuming process by DHFR [74]. Therefore the supplemented amino acids could lower the need for folate synthesis. The increase of DHF_2 under all supplementation conditions is a surprising result. Because of the energy intensive process to convert DHF to THF, all DHF glutamations should increase along with the decrease in THF concentrations. Why this does not occur is unclear. The increase of DHF_2 specifically, and not DHF_1 or DHF_3 to the same extent, could be due to different affinities for polyglutamated forms of THF in reactions such as MS or SHMT [75].

2.3.2 Mathematical modeling of *E. coli* folate:

The estimated Vmax values of the FPGS equation converting THF_2 to THF_3 and for the DHF_n sink were the most stable across all supplementation conditions. THF_2 and THF_3 do not hold the same quantitative relationship across the time course for all supplementation conditions, and DHF follows a similar pattern across all supplementation conditions. The model replicates a similar pattern in all scenarios: a major change in concentration within the first few minutes of TM addition, and stabilization of concentrations afterward. In every scenario that was modeled, the drop in THF_3 is significant (Figure 7, supplementary Figures 1-3). This is due to the massive increases in DHF_1 and DHF_2 that are seen in each scenario. We were not able to ascertain

the individual contributions of DHF polyglutamates to the increase in THF_3. However, while DHF experiences a severe perturbation in concentration very quickly, usually settling in to nearly final concentration within one minute, THF_3 shows a gradual change in concentration across all scenarios. This indicates either a structural buffering within the folate pathway to perturbations, or simply that the full effect of the perturbation takes a significant amount of time to propagate to all metabolites. Another interesting feature is that for all scenarios except GIMT supplementation, DHF_3 appears to return to a very similar concentration as what it was at time zero, before TM is added into the reaction chamber.

2.3.3 DHFS activation:

The enzyme acceleration model is a simple mathematical model of how enzyme activation could be exploited to achieve a bacterial disruption similar to that of an established antibiotic. It would not have been possible without the discovery that DHF inhibits FPGS [1]. This approach would probably work better when combined with TM and sulfamethoxazole, especially since there is a separate enzyme that converts DHF to THF, folM, which is less sensitive to TM [76, 77]. However sulfamethoxazole inhibits conversion of pABA into DHP, which is converted into DHF by the enzyme DHFS. If sulfamethoxazole were used, DHP supplementation would be necessary as well. More detailed experimentation and mathematical models would clarify whether this approach would be an effective treatment, but the presented model is a first step. The full

spectrum of enzyme-metabolite interactions in the *E. coli* folate pathway has not been established, and more exploration could yield more antibiotic targets.

3. Homocysteine Considerations on *E. coli* Stress

3.1 A Homocysteine

The following work explores the idea that L-HCY may actually function as a nutrient under certain conditions, and that its reputation as a metabolic stressor may be slightly oversold in the literature. Our experiments indicate that a more nuanced approach to L-HCY should be taken in the future, and that experiments on this metabolite should be carried out at far greater parameters than have been done previously.

3.2 Homocysteine Materials and Methods:

3.2.1 Homocysteine Growth reagents and materials:

M9 Medium reagents were purchased from Sigma-Aldrich USA unless otherwise noted [49]. L-HCY and L-Met were purchased from Santa Cruz Biochemistry. Growth studies were carried out in a Honeycomb 2 growth plate, in a Bioscreen C growth machine (Bioscreen Company, Finland). OD measurements were carried out in a Shimadzu UV2401-PC Spectrophotometer.

3.2.2 *E. coli* growth:

Unless otherwise indicated, strain *E. coli* MG1655 (Yale Stock Center) was used in all experiments. *E. coli* were grown overnight in 0.04% glucose M9 medium unless otherwise indicated, then diluted into individual Honecyomb plate wells for large scale growth assays or baffled Erlenmeyer flasks for proteomics experiments. For Honeycomb

plates, inoculates were placed into 1:20 inoculate:media ratios for a total of 200 μL growth solution. Erlenmeyer flasks were filled to a 1:8 ratio of growth media:air, with a total of 50 mL growth media. Erlenmeyer flasks were shaken at 225 RPM, and Honecyomb plate was shaken at equivalent RPM in the Bioscreen C growth device. All cultures were grown in 0.4% or 0.04 % glucose M9, or LB, at 37C. OD measurements at 600 nm were carried out either by Bioscreen C at 10 minute intervals, or with a Shimadzu optical density reader. At target OD's, samples were split for metabolomics and proteomics analysis. Cells were harvested by the rapid addition and mixing of 1:3 ratio mixing of bacterial culture into ice-cold 0.9% (w/v) NaCl, following the protocol of Halliday et al. 2010 [78]. Cell extracts were frozen at -80°C until used for proteomics analysis.

3.2.3 Proteomics – extraction, sample prep, resolution, and targets:

All data were taken in biological triplicate, whether for growth or for proteomics analysis. Frozen *E. coli* pellet samples in 0.9% NaCl storage solution were delivered to the Duke University School of Medicine Proteomics Core Facility in 1.5 mL Eppendorf tubes. Samples were thawed on ice and centrifuged at 14,000 rpm at 4°C for 15 minutes. Storage solution was pipetted off from each one and kept until completion of study. Pellets were rinsed with 200 μL of 50 mM ammonium bicarbonate, vortexed briefly, and centrifuged again for 5 minutes. The supernatant was then removed and 100 μL of 0.25% RapiGest (Waters Corp.) in 50 mM AmBic was added on top of the cell pellet for

protein solubilization. Each sample was probe sonicated at power level 3 for 3 bursts at 5 seconds/burst, storing on ice between bursts. Samples were then heated at 50°C for 20 minutes. Samples were again centrifuged for 5 minutes and protein concentration was measured by total protein assay (mini Bradford measured at 595 nm, Bio-Rad, Inc). 50 μg from each was taken out and normalized to the lowest concentration with 0.25% RapiGest. 2500 fmol of each stable-isotope labeled peptide (JPT, Inc.) for the 5 targeted proteins and ADH as internal standard were spiked in. Samples were then reduced in 10 mM dithiothreitol (VWR, VW1506-02), alkylated in 20 mM iodoacetamide (Calbiochem 407710), and digested with sequencing grade modified trypsin (Promega V5111) at a 1:50 ratio of trypsin to total protein (standard in-solution digestion protocol at (http://www.genome.duke.edu/cores/proteomics/sample-preparation/). After digestion overnight, samples were acidified to 1% trifluoroacetic acid/2% acetonitrile and heated for 2 hrs at 60°C to hydrolyze Rapigest, and spiked with 50 fmol Mass PREP ADH digestion standard (Waters, 186002328) per microgram of total protein. Samples were then centrifuged at 15,000 rpm for 5 minutes and the supernatants were pipetted into total recovery LC vials (Waters Corp.). A pooled sample was made by combining an equal volume from each of the samples. For a subset of samples, an alternative collection method was attempted, to ascertain differences in protein retention. This methodology employs a methanol/glycerol based quenching fluid [79]. Proteins were assayed as

absolute concentration by liquid chromatography-tandem mass spectrometry under various control growth conditions and two optical densities per condition.

Each sample was analyzed by injecting approximately 1 μg of total digested protein onto a 75μm x 250 mm BEH C18 column (Waters) and separated using a gradient of 5 to 40% acetonitrile with 0.1% formic acid, with a flow rate of 0.4 μL/min, in 30 minutes on a nanoAcquity liquid chromatograph (Waters). Electrospray ionization was used to introduce the sample in real-time to a Xevo triple quadrupole mass spectrometer (Waters). The selected reaction monitoring (SRM) method targeted 10 peptides from the proteins of interest - 2 peptides each to METE, METJ, METH, METR, and RPOS – plus 5 peptides to ADH, both stable isotope-labeled and label-free. The pool sample was run 4 times across the sample queue whereas all other samples were run in singlicate. Data from all runs was loaded into a freeware program called Skyline (https://brendanx-uw1.gs.washington.edu/labkey/project/home/software/Skyline/begin.view), and the peak areas from light and heavy versions of each peptide were integrated. Results were imported directly into Excel and a fmol/μg protein amount was determined by single point stable-isotope labeled calibration, simply multiplying the light:heavy peak area ratio to the amount of heavy-labeled peptide injected (50 fmol).

3.3 Homocysteine Results:

3.3.1 Growth response to HCY:

We found that concentrations of 1 mM and above HCY severely inhibit growth, whereas concentrations below 0.1 mM have little effect on growth under 0.4% glucose conditions and an initial culture optical density (OD) of 0.065 (Figure 10A). We also compared the effect of initial optical density and HCY dose on time for culture to achieve a cutoff optical density of 0.16. We found that HCY concentration is a stronger predictor of time to achieve OD = 0.16, under 0.4% glucose supplementation conditions (Figure 10B).

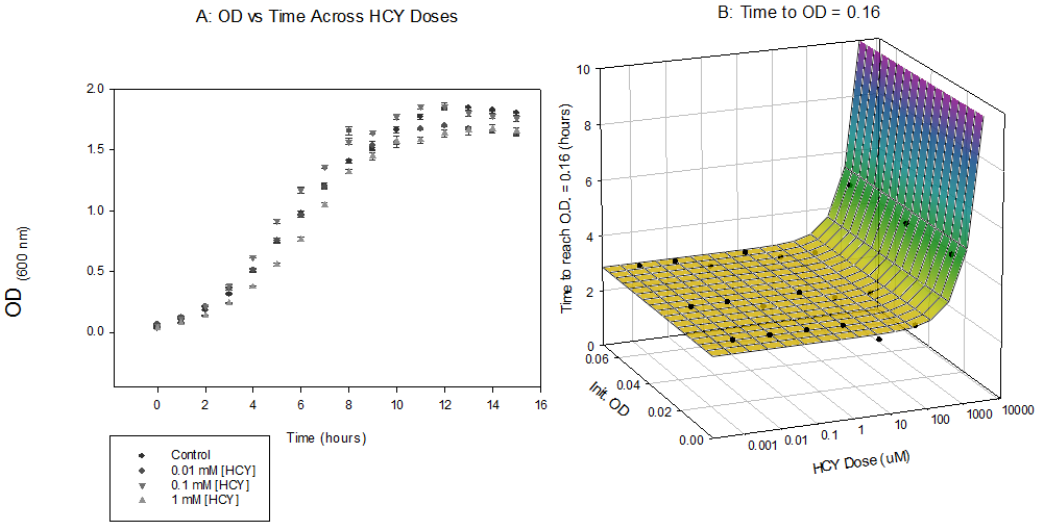

Figure 10: *E. coli* growth:

A: With broader sampling of HCY doses, we show low HCY doses that create no delay of growth and that high doses (1 mM and above) delay recovery from growth in the 0.4% condition (growth data for 0.04% not shown). B: HCY dose is

more influential than initial optical density for determining time at which a culture achieves target optical density with respect to control (0.16) for the 0.4% glucose condition.

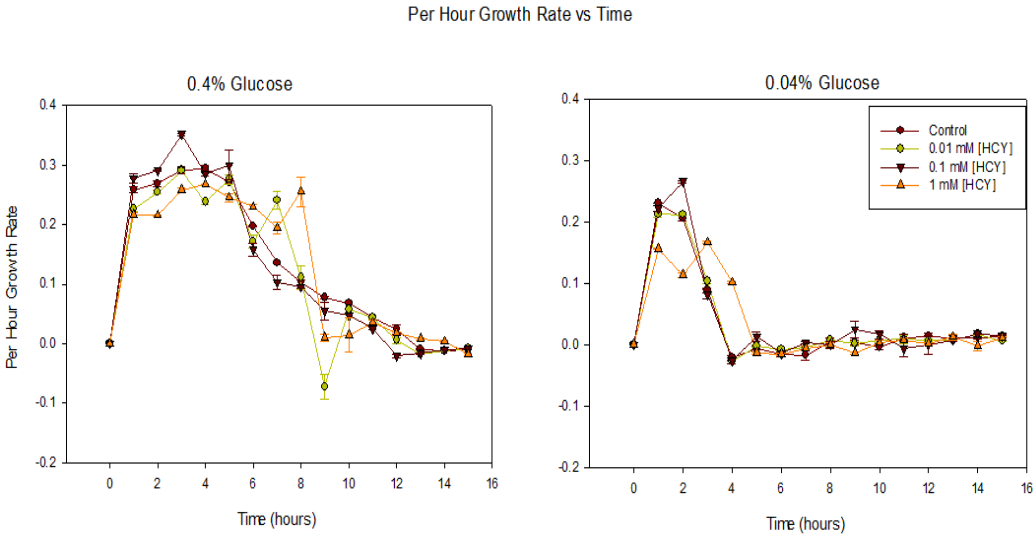

Figure 11: Growth rates of *E. coli* under varying HCY and glucose conditions: A (left): 0.4% glucose conditions lead to a series of HCY concentrations creating a slight acceleration in growth rate, but also a delay in achievement of maximum growth rate. B (right): 0.04% glucose conditions led to lower overall growth, and a narrowing of growth rate variations due to HCY dosing, from the control. Under both conditions, 0.1 mM led to an increase in growth rate from the control, making it a useful target for further study. The pattern of low doses leading to a slight decrease in growth rate, and doses in the 1 mM range and above leading to a large decrease in growth rate, with 0.1 mM leading to an increase, is seen in both glucose conditions.

Table 1: Maximum Growth Rate Changes from control with glucose and HCY

Percent Change of Max Growth Rate from Control Condition		
[HCY Dose]	**0.4% Glucose**	**0.04% Glucose**
0.1 mM	17% Increase	14% Increase
1.0 mM	24% Decrease	47% Decrease

A 0.1 mM dose increases maximum growth rate with respect to control in both 0.4% and 0.04% glucose growth conditions. 1 mM HCY decreases maximum growth rate from the control in both conditions.

Certain HCY doses such as 0.1 mM HCY result in a higher growth rate after recovery than control in both 0.4% glucose and 0.04% glucose supplementation. The 0.4% glucose condition experiences an average 17 percent increase in maximum growth rate from the control growth rate when supplemented with 0.1 mM HCY, whereas 0.04% glucose condition experiences a maximum growth rate increase of 14%. The response at 1 mM HCY dose causes an average 24 percent difference drop in maximum growth rate in the 0.4% glucose supplementation, while causing an average 47 percent difference drop in maximum growth rate for 0.04% glucose supplementation (**Error! Reference source not found.**). A delay of growth is not always linked to a decrease in maximum growth rate with respect to control (Figure 11). 0.1 mM treatment of HCY with 0.04% glucose causes an increased maximum growth rate but also a one hour delay from the control to achieve that rate, while in 0.4% glucose conditions the 0.1 mM growth rate is actually achieved one hour faster than the control. 1 mM HCY treatment causes delay to

achievement of max growth rate under both glucose conditions. Doses of HCY under 0.1 mM appear to cause no significant delay in growth recovery from control conditions (data not shown).

3.3.2 Proteomics of response to HCY:

Table 2: Average percent difference of Met Cycle proteins from control conditions to conditions of 0.1 mM HCY, with different glucose supplementation

Target Protein	*M9 0.4% Glu, Low OD*	*M9 0.04 % Glu, Low, OD*
METE	-40.82	82.09 *
METH	-48.38	9.63 *
METJ	-41.35 *	-12.58 *
METR	-57.32	10.99 *
RPOS	-60.02	37.25*

A Kruskal-Wallis (KW) statistical test was carried out on protein concentration averages. Averages that failed the KW test are marked with *. 0.4% glucose supplementation appears to result in a general downregulation of Met cycle proteins and RPOS after exposure to HCY. In the 0.04% glucose condition, we see no statistically significant change in protein concentrations. No protein including RPOS passes KW test in the 0.04% glucose condition, indicating that with regards to protein concentrations, *E. coli* appears to not feel any effect of HCY under the

0.04% glucose condition despite clearly showing an increased growth rate at the macro level.

METJ, METR, METE, METH, and the stress response protein RPOS were assayed as described in Methods. RPOS is a central stress response protein induced when *E. coli* enters stationary phase [80]. We show protein concentration changes under conditions of HCY exposure in M9 growth media, with 0.4% and 0.04% glucose supplementation (Table 2). At an optical density of 0.065, we dosed *E. coli* growing in both glucose conditions with 0.1 mM HCY and assayed protein concentrations 40 minutes after exposure. In the 0.4% glucose condition, all target proteins showed downregulation, with METJ failing to show statistical significance using a Kruskal-Wallis test. However, in the 0.04% glucose condition, all target proteins were upregulated but failed tests for statistical significance.

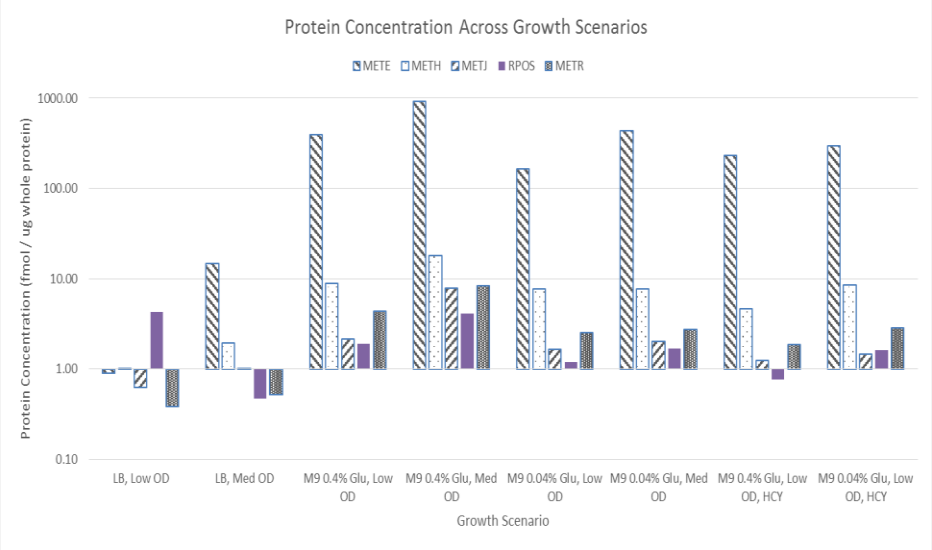

Figure 12: Average Protein Concentration at femtomol / µg whole protein:

The average protein concentration protein targets is presented under various growth scenarios. METE shows significant change in concentration. METE undergoes an approximately 43,000% difference between average concentration in growth condition of LB at O.D. = 0.065, to M9 at the same optical density. Even between two cell densities in LB media (O.D. = 0.065 and 0.26), METE percentage difference is approximately 1500. When sampled under conditions of HCY media supplementation, differing glucose concentrations in growth media elicit a different response. Under 0.4% glucose conditions in M9 defined media, exposure to 0.1 mM HCY drives down met cycle proteins. However, under 0.04% glucose conditions, METE, METH, and METR increase in concentration upon similar HCY exposure, compared to their respective controls. The 0.4% glucose instance appears to indicate a stress response similar to what is found in Fraser et al. [26]. The 0.04% glucose condition appears to show little change in METR and METH, but a significant increase in METE from control, which partially agrees with Cai et al. [64].

3.3.3 Protein concentration changes across a broad range of nutrient conditions:

The enzyme METE undergoes drastic changes in concentration between control nutrient conditions (LB, M9 0.4% glucose, M9 0.04% glucose, Figure 12). For example, concentration percent difference from LB to M9 0.4% is approximately 43000. Other targeted proteins do not show such extreme changes. Linear regression of METE and

METR, yielded a high coefficient of determination (R2 = 0.86, Figure 13A). METE and METH also showed a high positive coefficient of determination with R2 = 0.79. RPOS concentration was compared with all methionine cycle proteins. METJ and RPOS yielded a coefficient of determination of R2 = 0.06. Principal component analysis shows that RPOS is not correlated with methionine cycle proteins (Figure 14). A highly unexpected result was the positive relationship of METJ and METR, with a coefficient of determination of R2 = 0.56 and an RMSE/DV comparable to METE/METR correlations. METJ is widely thought to be a repressor of METR. However our data, taken over a broad nutrient parameter space, shows a positive relationship of the concentrations of METJ and METR.

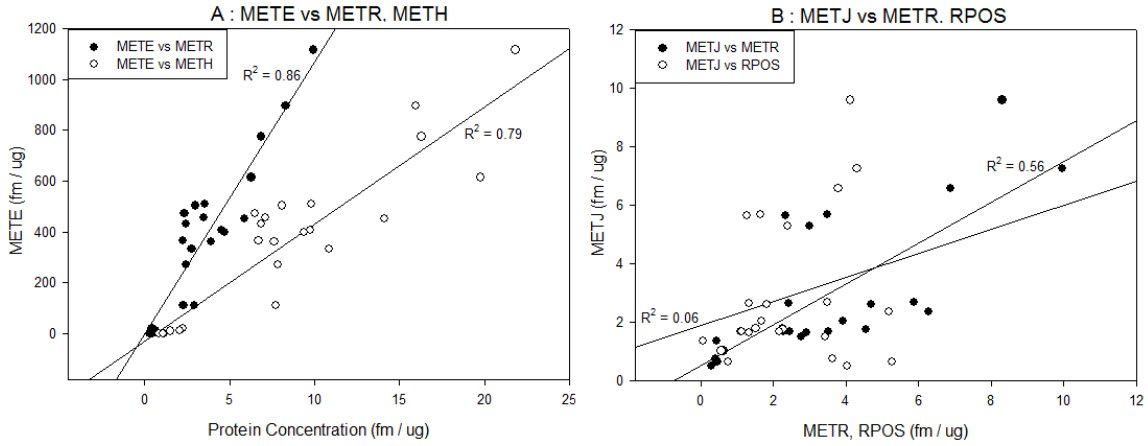

Figure 13: Met Cycle protein concentration linear regressions

A: Two linear regressions of MET cycle proteins are shown, using concentration data from all growth conditions except under HCY supplementation. METE and METR have the highest R squared and lowest RMSE/DV (RMSE/DV not shown).

METE also has a high R squared with METH. B: METJ correlate best with METE with an R2 of 0.70 (not shown due to scaling). METJ correlates well with METR as well, seen in contrast to RPOS, which correlated poorly with all MET cycle proteins. While higher degree polynomials do sometimes increase R squared significantly (Figure S1) we use the simplest parameters possible for this study, to come to the most conservative conclusions about the data.

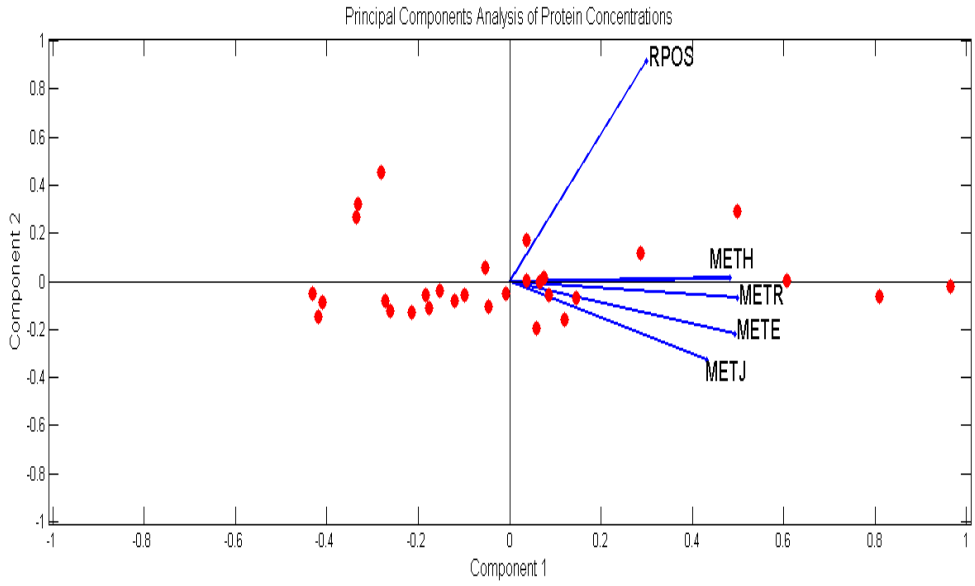

Figure 14: Principal Components Analysis of all assayed proteins

The projection of the MET and RPOS variables onto the principal component biplot shows the two variables fall mostly on separate axis, indicating variations between the two sets of proteins are nearly uncorrelated. We see the MET family proteins are mostly interchangeable in relation to RPOS. RPOS is seen mostly on PC2, indicating that RPOS is fairly uncorrelated with methionine cycle protein

response. Data is z-score adjusted to avoid fluctuations in METE overwhelming the PCA.

3.4 Homocysteine Discussion:

3.4.1 Growth under HCY:

We show that the recovery dynamics of HCY is more complex than previously reported. We chose two growth conditions as controls: M9 minimal medium with 0.4% glucose and 0.04% glucose, to test nutritional dependency of response to HCY exposure. We also chose concentrations of HCY that are below those used in previous studies to explore the minimum concentration required for an alteration in growth.

Maximum control growth rate under 0.4% glucose is approximately 74% faster than growth under 0.04% glucose supplementation, with maximum growth rate for each control condition being 0.384 and 0.22 respectively. The increased growth rate with respect to control upon HCY exposure at 0.1 mM HCY for both glucose conditions is a surprising and previously unreported result. Data for the 1 mM HCY dose for both nutritional conditions is in agreement with previous reports, showing a reduction in growth rate and a delay in achievement of maximum growth rate. The 0.1 mM [HCY] and 0.04% condition experiences both an increase in maximum growth rate and a delay in achieving that rate with respect to control conditions, pointing to subtle dynamics of recovery from stress and response to HCY.

There are possible reasons for the responses shown in this study. Tweeddale et al. found that under extreme growth depression by glucose limitation, certain metabolite pools such as glutathione can change significantly [81]. The change in glutathione could have an effect on the response to HCY. However, our M9 growth conditions used glucose supplementations far higher than the Tweeddale et al. study [81]. As to the faster growth under 0.1 mM HCY, we do not have an explanation for this behavior, other than perhaps that this dose of HCY is exploited by *E. coli* as a nutrient via conversion to methionine by methionine synthase (METE) while simultaneously not at a high enough a concentration to be toxic and inhibit growth.

3.4.2 Proteomics across nutrient conditions:

Methionine cycle protein concentrations were assayed under multiple growth and optical density conditions to gain a broader insight into the regulation of the methionine cycle via relationships in protein concentration. METE, METR, METJ, METH and the stress response protein RPOS were measured. Earlier studies of protein concentration have focused on narrow parameter spaces of nutrition and cell density [63-66]. The proteomics data is a set of clear quantitative relationships that can provide insight into *E. coli* methionine cycle behavior in vivo, as it may behave in nature, where bacteria face an environment with extreme spatial and temporal variation in nutrient conditions. The data set also provides a baseline set of information on how this specific

pathway adjusts to extremely different nutrient conditions. This information is useful for researchers aiming to build models of how the methionine cycle behaves in nature.

However target protein concentrations are significantly different between LB and M9 growth conditions. Met cycle protein concentrations change relatively little between scenarios of M9 growth medium with 0.4% glucose to 0.04% supplementation. METE is the most variable of the proteins across conditions. The concentration relationships of target proteins shown in Figure 13 mostly agree with the observations of Cai, Maxon, and Marincs, et al. [61, 63-65]. However some protein relationships such as METJ and METR show relationships that, at first look, disagree with these studies. For example, METJ is categorized as a repressor of *metR* in S. trymithipruum and *E. coli*, in both defined and rich media (M9 and LB, respectively) [56, 63, 65, 69]. We propose that our data showing a positive slope on the linear regression of METJ and METR (Figure 13B) is an instance of Simpson's Paradox, a phenomenon in which local samplings show one relationship between system elements, but a global sampling shows a different if not opposite relationship [82]. Simpson's Paradox is a clear phenomenological explanation for why differing sampling strategies have yielded contradictory protein concentration relationships.

3.4.3 Proteomics under HCY:

Cultures grown in M9 under 0.4% and 0.04% glucose were exposed to a dose of 0.1 mM HCY. The 0.4% glucose condition displayed a decrease of Met cycle proteins

with respect to the control condition (Table 2). Earlier work showed that exposure to 0.5 mM HCY lead to downregulation of Methionine cycle mRNA, with metE mRNA downregulated by a factor of 2.4 [26]. This was attributed to a stress response to HCY. In our study, METE protein only decreased by 40%, indicating a significant difference between mRNA and protein downregulation.

4. Conclusions and Future Work

4.1 Conclusions:

The presented experiments show an unexpected acceleration of *E. coli* under certain conditions of L-HCY exposure. In addition, this study broadens understanding of methionine cycle regulation, showing a different relationship between METJ and METR at broad nutrition parameters than what is seen at narrower nutrition conditions. The results point to a more complex picture of met cycle regulation, and more closely describe the possible functioning of this system in a natural environment.

4.2 Future Work

4.2.1 Building better models of *E. coli* folate metabolism:

The mathematical model presented here can be vastly improved with a finer accounting of tetrahydrofolate analogues. The data set generated by Kwon et al. tracks individual analogues, which were compressed into one large variable of THF_n in the current mathematical model and the previous one. In addition, not holding Vmax and flux parameters constant during the entire simulation run may help create a better set of simulation fits. Lastly, a more detailed accounting of cofactor influence on folate function may greatly help with simulation efforts, since Kwon et al. have noted that NADH and other cofactors fluctuate significantly when *E. coli* is exposed to TM [1, 4]. With regards to amino acids that are tied to folate interconversions such as SAM and MET, experimental efforts in the future should focus on gathering absolute

concentrations of these targets instead of relative concentrations. The behavior of the folate pathways is clearly very dependent on amino acid concentrations, and an accurate set of concentration data would prove very useful in understanding the regulatory architecture of the *E. coli* folate network.

4.2.2 Approaching drug design with an optimization mindset:

Employing acceleration of an enzyme to disrupt metabolism instead of inhibition allows us to more easily conceptualize an enhanced approach to drug development: that of ultra-fine control of a biological system, exploiting simultaneous acceleration and inhibition of biological elements (transcriptional elements, enzymes, and metabolite dosing) in a cell. This is opposed to the approach of using one chemical treatment for one disease state. While some methods are being developed that are similar to this approach, such as using mRNA injections in subcutaneous tissue, the manipulations are not at the proposed scope and depth of control [83, 84]. Consider a human system (Figure 15A). For simplicity, we consider two cell types, 1 and 2 in a variety of disease and non-disease states. Initially, both behave as expected. For the purposes of this study the difference in cell types can be quantified as a set of differences in homeostatic fluxes, relationships between enzymes and regulatory elements, and metabolite concentrations. Consider that Cell Type 1 initially is in the Control state (C1). The sister cell type 2 is also in a control state (C2). C1 experiences a malfunction in an enzyme or a metabolite flux. We then have a new state that shifts cell type C1 into a disease state, which we label as

type D1 (Disease 1). For the sake of simplicity, cell type D2, which is formerly type C2, is not currently experiencing any malfunctions.

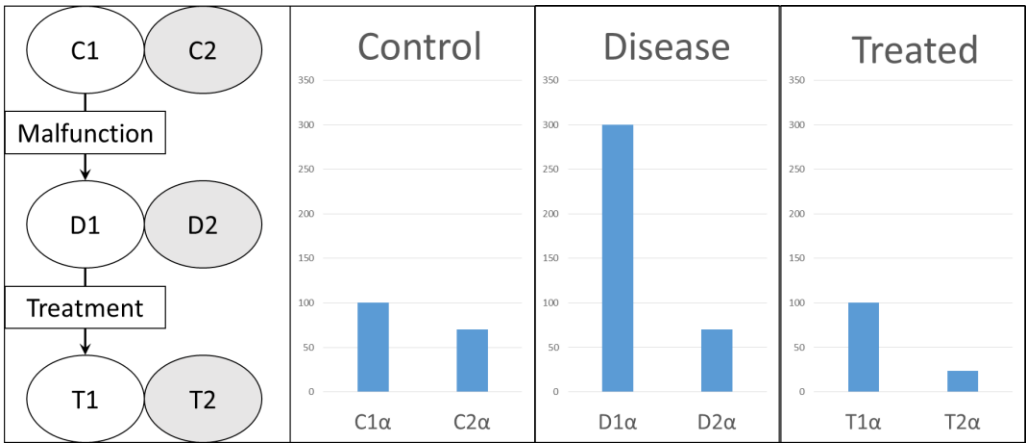

Figure 15: A, B

Modern treatment approaches aim to turn target cells such as D1 into a third type, T1 (Treated 1), which is a drug treated version of D1. The aim is to get cell type T1 as close the original C1 state as possible. A major understanding of how side effects arise is that downstream effects of initial cell elements affected by drugs cause unintended disruptions. However this statement ignores another kind of side effect. Side effects can also arise when the drug or treatment that is targeting type D1 affects cell type D2 as well, and turns it into T2, a cell that is adversely affected by the treatment. The ideal objective is to take a D1 to T1 to C1 without creating a T2, or minimizing the effect that the, "Type 2," non-target cells experience. Currently, proper targeting of drug delivery is

a major focus for avoiding side effects via T2. But the strategy of targeting can be improved upon in avoiding unintended consequences.

4.2.3 Distributed Drug Design Framework

The proposed framework rests on three elements:

1. Mathematical modeling the behavior of the relevant pathways in the target cell in normal, malfunctioning, and treated states via mathematical models.

2. Mathematical modeling of non-target cells under normal, malfunctioning, and treated states via mathematical models that account for how side effects, if any arise.

3. Exploiting multiple points of attack within target cells, while monitoring the effect of those same points of attack on non-target cells, to find an optimum treatment strategy.

Elements 1 and 2 allow us to understand how to a high degree how the cell types in various states behave, and to quantify the differences between cell types and disease states. Let us consider a simple example.

a. We consider a reaction rate α in the target cell C1. Under normal homeostatic conditions, α runs at 100% (Figure 7B). Under a diseased state, the rate of α in cell type C1 goes up three-fold, causing a disruption across the cell, converting it to type D1.

b. We now quantify the non-target cell. In the non-target C2 this same rate α is at 70% of that in C1, which is one of the many rate differences that helps define C2 as a

cell type different from C1. For simplicity, in the disease state, the non-target cell's rate α is still at 70%.

The most obvious strategy is to lower rate α in cell type 2 by 66%, leading to cell type 2's return to its original rate. If the treatment is not targeted specifically to C2 properly, the effect on rate α in cell type D2 can likely, can be cut by 66% as well. This will possibly severely hamper C2. In order to affect D1 strongly enough to actually bring it closer to the C1 state, a single therapeutic agent will have to be considerably potent, and will naturally lead to a side effect when implemented. If one therapeutic agent is sure to cause side effects, multiple simultaneous points of attack may provide a lower cost solution. Recall the enzyme acceleration approach. A similar, but smaller effect of inhibiting THF_{i+1} concentrations was achieved by targeting a different enzyme, DS. We advocate expanding this idea to include several simultaneous targets with different therapeutic agents. The purpose of using a larger set of targets is that they can approach a lowering of rate alpha (or a more roundabout solution) from multiple angles, with a net cost to cell types 2 that is lower than the cost from one potent therapeutic agent.

When multiple fluxes or connections are simultaneously manipulated, a treatment regime can possibly be created for D1 which does not disrupt D2. There is an explicit possibility that several small treatments could also interact with each other to perturb D2 even more than the original treatment approach. By not focusing solely on a strong manipulation of α, and instead simultaneously attacking other elements along

with α, the probability that several small modulations of Cell Type D1 will end up not perturbing Cell Type D2 increases. A distributed approach that targets multiple enzymes simultaneously lowers the need for each chemical agent to have a strong effect. A lower threshold for effect can, if structured properly, lead to a lower set of side effects. This is because multiple small effects can, by definition, lead to an additive effect that can be crafted more carefully than one large effector. That disease states can be considered basins of attraction that are difficult to move out of without a strong effector [85]. Acknowledging this, there is still benefit in a distributed approach on top of a lower dose of a single strong therapeutic agent. We propose that drug formulation begin with a multiple low intensity effector, distributed treatment strategy in mind. Omics and mathematical modeling research can be planned with the explicit intent of finding multi-pronged optimum strategies. Therapeutic agents that were previously disregarded because they were low in efficacy could be reconsidered as instrumental to this approach. However, finding optimal treatment strategies may not be possible if non-target cells are not assayed with the same data resolution. Regarding approaches to antibiotic development with multiple manipulations, Bonhoeffer et al. show that deployment of sub-optimal efficacy of vaccinations can be useful in cases where drug-resistant infections are prevalent [86, 87].

4.3 Building better experiments of E. coli metabolite stress:

We propose simultaneous sampling of bacterial growth, absolute concentrations of metabolites, proteins and gene expression in multiple interconnected pathways at high fidelity, possibly with LCMS/MS methods. These kinds of data could be simultaneously gathered under control conditions, large perturbations (meaning large doses of metabolites such as HCY), and in times of growth recovery, where applicable. The reason for this approach is to get high fidelity data that could be used in math models to uncover the subtle logic of gene regulatory networks in a dynamic manner. Genes, proteins, and metabolites all interact with each other, and gathering data on each of these layers of information simultaneously will allow for more clear relationships to be built. We also propose investigation for the existence of micro-perturbations in microorganisms, which we define as pathway-level physiological changes to external stimuli that do not manifest themselves in the growth response of a microorganism. Our data showing that similar responses at the growth level do not correspond to similar responses at the protein concentration level suggest that information processing in microorganisms is a complex, multi-layered process, but one that can be elucidated with proper experimentation. A major objective would be to assess to what extent bacterial and microorganism systems have a homeostatic buffering akin to what is seen in multicellular organisms. More specifically, we propose building more broad associations between protein and mRNA concentration targets in the MET cycle, and

exploring the exact time-course mathematical relationships between METJ and each of its targets, each of which are further along on the methionine production pathway [60]. If the pathway is indeed a linear progression of metabolites from ASP to MET, then we can assume a relationship among location in the pathway and METJ target. A fine-tuned exploration of the relationships between metabolites, gene expression, and protein concentration, in time course, will reveal how the system operates in real-time, and will undoubtedly create more opportunities for antibiotic therapeutics.

5. Supplementary Figures

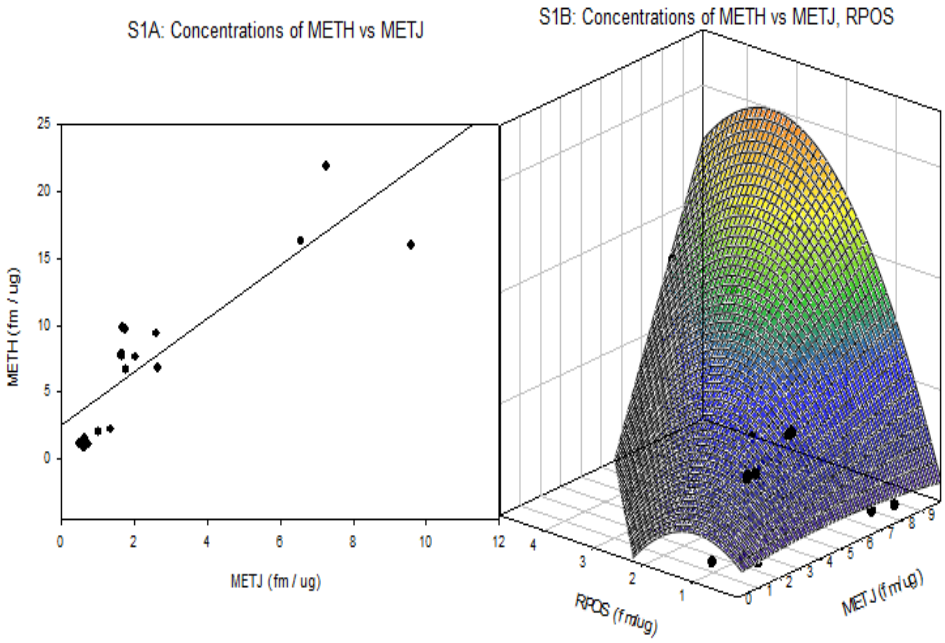

Figure S1: METJ and RPOS may be predictive of METR and METH at high dimensions

(A) METJ and METH correlate fairly poorly when compared to their other MET family proteins, with an R2 of 0.4, using a one degree polynomial. Increasing the polynomial degree does not improve the R2. RPOS and METH also do not correlate well. (B) When METJ, RPOS, and METH are placed in the X, Y, and Z coordinates, the R2 when METJ is changed from a 1 degree to 2 degree polynomial changes from 0.50 to 0.85. A similar result occurs with METJ, RPOS, and METR, with an R2 leap from 0.62 to 0.86. An exhaustive combinatorial search revealed no such improvement in any other combination of three-component polynomial regression. Many of the R2 values at three dimensions

are not indicative of any real increase in predictive power from the prediction of one protein to another (data not shown). Increasing the dimensionality of RPOS in the METJ, RPOS, METR/METH cases does not increase the R2 from the one-degree X/Y polynomial fit condition. As expected, placing RPOS as the resultant (Z axis) universally results in R2 of 0.2 or below. The MET cycle proteins cannot predict RPOS, even when paired together, yet RPOS may aid in predicting some MET cycle proteins, with METJ. We introduce this data to show how higher degree polynomial expressions may reveal interesting dynamics, but we also urge caution against interpreting the results too liberally.

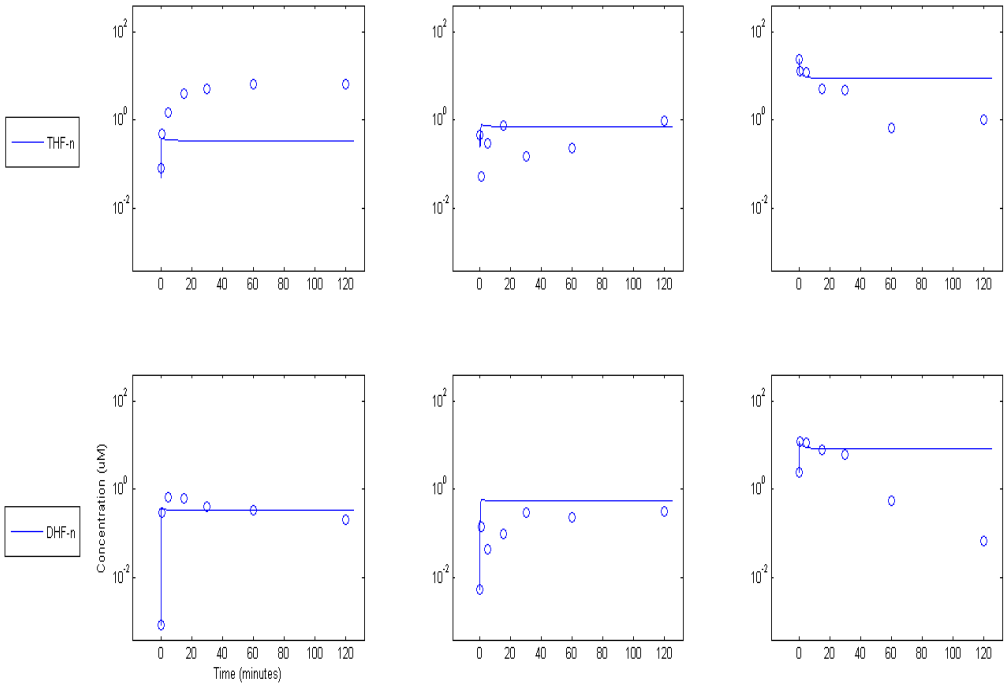

Figure S2: Simulation and Experimental Data for GIMT Supplementation

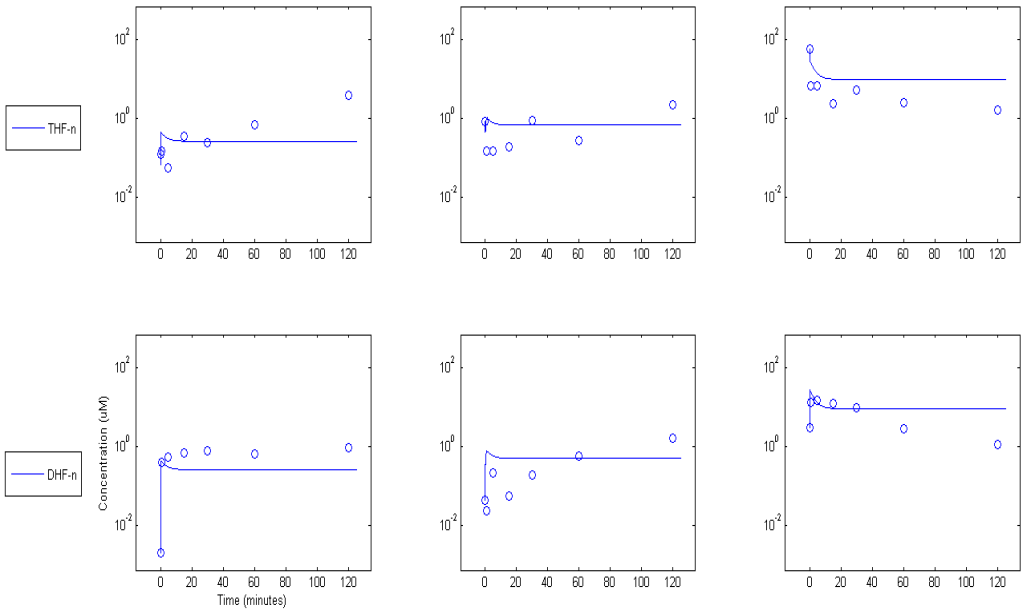

Figure S3: Simulation and Experimental Data for GIM Supplemenation

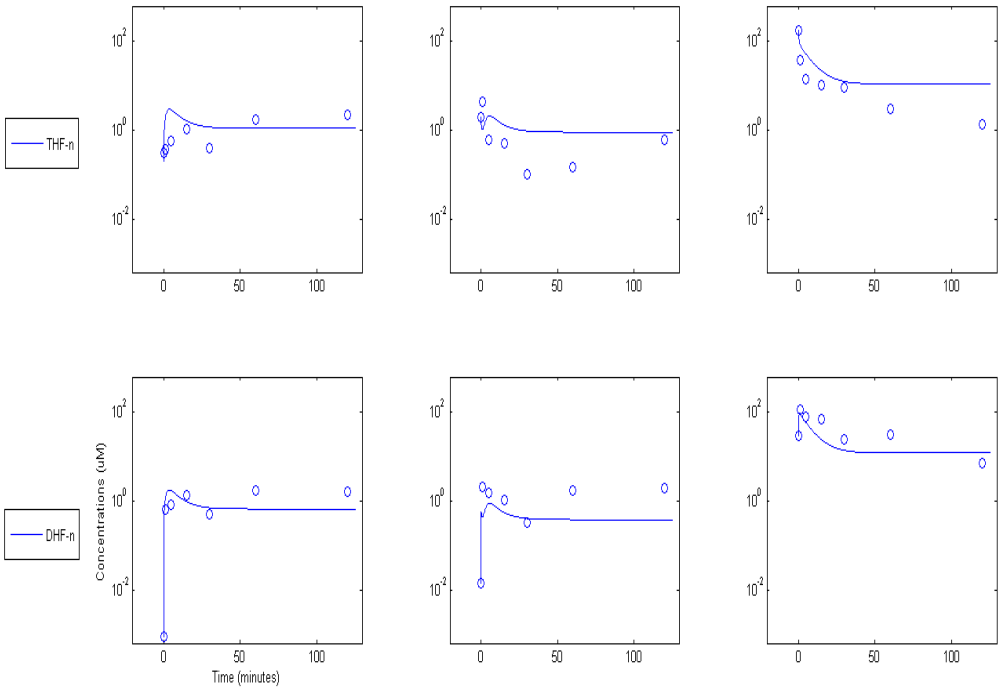

Figure S4: Simulation and Experimental Data for Inosine Supplementation

Appendix A: Folate Model Differential Equations

ODEs:

d(THF2)/dt = 1/unnamed*(-ReactionFlux2 + ReactionFlux4 - ReactionFlux5)

d(THF1)/dt = 1/unnamed*(-ReactionFlux1 - ReactionFlux4)

d(DHF2)/dt = 1/unnamed*(ReactionFlux2 - ReactionFlux8)

d(THF3)/dt = 1/unnamed*(-ReactionFlux3 + ReactionFlux5 - ReactionFlux7)

d(DHF3)/dt = 1/unnamed*(ReactionFlux3 - ReactionFlux10)

d(DHF1)/dt = 1/unnamed*(ReactionFlux1 + ReactionFlux6 - ReactionFlux9)

d(F1)/dt = 1/unnamed*(-ReactionFlux6 + ReactionFlux7 + ReactionFlux8 + ReactionFlux9 + ReactionFlux10)

Fluxes:

ReactionFlux1 = THF1Vmax*THF1/(THF1Km*(1+DHF1/THF1Ki)+THF1)

ReactionFlux2 = THF2Vmax*THF2/(THF2Km*(1+DHF2/THF2Ki)+THF2)

ReactionFlux3 = THF3Vmax*THF3/(THF3Km*(1+DHF3/THF3Ki)+THF3)

ReactionFlux4 =

((FPGS_Vmax_1*THF1/Km_1)/(1+DHF1/KI_1+DHF2/KI_1+DHF3/KI_1+THF1/Km_1+THF2/Km_1))

ReactionFlux5 =

((FPGS_Vmax_2*THF2/Km_2)/(1+DHF1/KI_2+DHF2/KI_2+DHF3/KI_2+THF1/Km_2+THF2/Km_2))

ReactionFlux6 = KINVmax*F1/(KINKm+F1)

ReactionFlux7 = K6*THF3

ReactionFlux8 = k5b*DHF2

ReactionFlux9 = k5a*DHF1

ReactionFlux10 = k5c*DHF3

Table 3: Parameter sets across scenarios

Parameter/Scenario	GIMT	GIM	Ino	No Supplement
K1	0.6255	1.8745	1.1145	0.9483
K2	0.9357	0.8565	1.1261	0.2370
k3	1.6918	1.5587	1.0089	1.5934
K6	0.2581	0.1114	0.1934	3.2745
k4a	0.6467	0.1802	0.5886	2.0452
k4b	1.7318	0.3967	1.8307	0.5944
k4c	0.2771	0.6615	1.5515	1.0368
k5a	2.2516	0.9682	3.7741	2.3630
k5b	1.1184	1.8136	0.6984	0.1859
k5c	0.3517	0.4414	2.1941	1.0044
KIN	0.5560	2.0659	0.0412	0.0475
FPGS_Vmax_1	1.3604	2.5923	1.8875	2.3566
FPGS_Vmax_2	1.7948	1.5935	1.6485	1.3975
k_Recycle_1	0.9193	0.3941	0.8505	1.1970
k_Recycle_2	1.0001	0.0227	0.0640	0.1190

Appendix B: Enzyme Acceleration Differential Equations

ODEs:

d(THFi1)/dt = 1/unnamed*(ReactionFlux4 - ReactionFlux5)

d(DHP)/dt = 1/unnamed*(ReactionFlux1 - ReactionFlux2)

d(DHF)/dt = 1/unnamed*(ReactionFlux2 - ReactionFlux3)

d(THFi)/dt = 1/unnamed*(ReactionFlux3 - ReactionFlux4)

d(Sink)/dt = 1/unnamed*(ReactionFlux5)

Fluxes:

ReactionFlux1 = k_source*Source

ReactionFlux2 = DSVMAX*DHP/(DSKM+DHP)

ReactionFlux3 = DHFR_VMAX*DHF/(DHFR_KM*(1+TM/TM_Ki)+DHF)

ReactionFlux4 = FPGS_VMAX*THFi/(FPGS_KM*(1+DHF/FPGS_Ki)+THFi)

ReactionFlux5 = k_sink*THFi1

Table 4: Parameter values for Enzyme Acceleration Model

Parameter values listed are under control conditions with 0 TM. DSKM was reduced to 1E-4 for "acceleration" model.

R_source	10.5
DSVMAX	200
DSKM	1
DHFRVMAX	200
DHFRKM	10
TM_Ki	0.004
FPGSVMAX	200
FPGSKM	1
FPGSKi	10
k_sink	20

Works Cited

1. Kwon, Y.K., et al., *A domino effect in antifolate drug action in Escherichia coli.* Nat Chem Biol, 2008. **4**(10): p. 602-608.

2. Gonzalez, J.C., et al., *Comparison of cobalamin-independent and cobalamin-dependent methionine synthases from Escherichia coli: two solutions to the same chemical problem.* Biochemistry, 1992. **31**(26): p. 6045-6056.

3. Taurog, R.E., H. Jakubowski, and R.G. Matthews, *Synergistic, random sequential binding of substrates in cobalamin-independent methionine synthase.* Biochemistry, 2006. **45**(16): p. 5083-91.

4. Kwon, Y.K., M.B. Higgins, and J.D. Rabinowitz, *Antifolate-induced depletion of intracellular glycine and purines inhibits thymineless death in E. coli.* ACS Chem Biol, 2010. **5**(8): p. 787-95.

5. Shane, B., *Pteroylpoly(gamma-glutamate) synthesis by Corynebacterium species. Purification and properties of folypoly(gamma-glutamate) synthetase.* Journal of Biological Chemistry, 1980. **255**(12): p. 5655-5662.

6. Shane, B., *1 Folate Chemistry and Metabolism.* Folate in health and disease, 2010: p. 1.

7. Drummond, J.T., et al., *Characterization of Nonradioactive Assays for Cobalamin-Dependent and Cobalamin-Independent Methionine Synthase Enzymes.* Analytical Biochemistry, 1995. **228**(2): p. 323-329.

8. Bognar, A., et al., *Folylpoly-gamma-glutamate synthetase-dihydrofolate synthetase. Cloning and high expression of the Escherichia coli folC gene and purification and properties of the gene product.* J Biol Chem, 1985. **260**: p. 5625 - 5630.

9. Bognar, A.L. and B. Shane, *[55] Bacterial folypoly([gamma]-glutamate) synthase-dihydrofolate synthase*, in *Methods in Enzymology*, D.B.M. Frank Chytil, Editor. 1986, Academic Press. p. 349-359.

10. Masters, P.A., et al., *TRimethoprim-sulfamethoxazole revisited.* Archives of Internal Medicine, 2003. **163**(4): p. 402-410.

11. Christensen, K.E. and R.E. MacKenzie, *Mitochondrial one-carbon metabolism is adapted to the specific needs of yeast, plants and mammals.* Bioessays, 2006. **28**(6): p. 595-605.

12. Christensen, K.E. and R.E. MacKenzie, *Chapter 14 Mitochondrial Methylenetetrahydrofolate Dehydrogenase, Methenyltetrahydrofolate Cyclohydrolase, and Formyltetrahydrofolate Synthetases*, in *Vitamins & Hormones*, L. Gerald, Editor. 2008, Academic Press. p. 393-410.

13. Leduc, D., et al., *Flavin-dependent thymidylate synthase ThyX activity: implications for the folate cycle in bacteria.* J Bacteriol, 2007. **189**(23): p. 8537-45.

14. Eschenbrenner, M. and M.S. Jorns, *Cloning and mapping of the cDNA for human sarcosine dehydrogenase, a flavoenzyme defective in patients with sarcosinemia.* Genomics, 1999. **59**(3): p. 300-8.

15. Lee, J.C., et al., *The prevalence of trimethoprim-resistance-conferring dihydrofolate reductase genes in urinary isolates of Escherichia coli in Korea.* Journal of Antimicrobial Chemotherapy, 2001. **47**(5): p. 599-604.

16. Dauber-Osguthorpe, P., et al., *Structure and energetics of ligand binding to proteins: Escherichia coli dihydrofolate reductase-trimethoprim, a drug-receptor system.* Proteins: Structure, Function, and Bioinformatics, 1988. **4**(1): p. 31-47.

17. Szegedi, S.S., et al., *Betaine-Homocysteine S-Methyltransferase-2 Is an S-Methylmethionine-Homocysteine Methyltransferase.* Journal of Biological Chemistry, 2008. **283**(14): p. 8939-8945.

18. Vedantam, G. and B.P. Nichols, *Characterization of a mutationally altered dihydropteroate synthase contributing to sulfathiazole resistance in Escherichia coli.* Microb Drug Resist, 1998. **4**(2): p. 91-7.

19. Blahna, M.T., et al., *The role of horizontal gene transfer in the spread of trimethoprim–sulfamethoxazole resistance among uropathogenic Escherichia coli in Europe and Canada.* Journal of Antimicrobial Chemotherapy, 2006. **57**(4): p. 666-672.

20. Huang, E.Y., A.M. Mohler, and C.E. Rohlman, *Protein expression in response to folate stress in Escherichia coli.* J Bacteriol, 1997. **179**(17): p. 5648-53.

21. Sangurdekar, D., Z. Zhang, and A. Khodursky, *The association of DNA damage response and nucleotide level modulation with the antibacterial mechanism of the anti-folate drug Trimethoprim.* BMC Genomics, 2011. **12**(1): p. 583.

22. Poole, K., *Bacterial stress responses as determinants of antimicrobial resistance.* Journal of Antimicrobial Chemotherapy, 2012.

23. Hesketh, A., et al., *Genome-wide dynamics of a bacterial response to antibiotics that target the cell envelope.* BMC Genomics, 2011. **12**(1): p. 226.

24. Lee, S., et al., *Targeting a bacterial stress response to enhance antibiotic action.* Proceedings of the National Academy of Sciences, 2009. **106**(34): p. 14570-14575.

25. Tuite, N.L., K.R. Fraser, and C.P. O'Byrne, *Homocysteine Toxicity in Escherichia coli Is Caused by a Perturbation of Branched-Chain Amino Acid Biosynthesis.* J. Bacteriol., 2005. **187**(13): p. 4362-4371.

26. Fraser, K.R., et al., *Global effects of homocysteine on transcription in Escherichia coli: induction of the gene for the major cold-shock protein, CspA.* Microbiology, 2006. **152**(Pt 8): p. 2221-31.

27. JAKUBOWSKI, #160, and H., *The Pathophysiological Hypothesis of Homocysteine Thiolactone-mediated Vascular Disease*. Vol. 59. 2008, Kraków, POLOGNE: Polish Physiological Society. 13.

28. Jakubowski, H., *Molecular basis of homocysteine toxicity in humans.* Cellular and Molecular Life Sciences, 2004. **61**(4): p. 470-487.

29. Blom, H.J. and Y. Smulders, *Overview of homocysteine and folate metabolism. With special references to cardiovascular disease and neural tube defects.* J Inherit Metab Dis, 2011. **34**(1): p. 75-81.

30. Petti, A.A., et al., *Survival of starving yeast is correlated with oxidative stress response and nonrespiratory mitochondrial function.* Proceedings of the National Academy of Sciences, 2011.

31. Hesse, H., et al., *Current understanding of the regulation of methionine biosynthesis in plants.* J Exp Bot, 2004. **55**(404): p. 1799-808.

32. Matthews, R., *One-carbon metabolism.* Escherichia coli and Salmonella: Cellular and Molecular Biology, 1996. **1**: p. 600 - 611.

33. Roje, S., *S-Adenosyl-l-methionine: Beyond the universal methyl group donor.* Phytochemistry, 2006. **67**(15): p. 1686-1698.

34. Avila, M.a.A., et al., *Methylthioadenosine.* The International Journal of Biochemistry & Cell Biology, 2004. **36**(11): p. 2125-2130.

35. Singh, V., et al., *Femtomolar transition state analogue inhibitors of 5'-methylthioadenosine/S-adenosylhomocysteine nucleosidase from Escherichia coli.* J Biol Chem, 2005. **280**(18): p. 18265-73.

36. Tavender, T., et al., *LuxS-independent formation of AI-2 from ribulose-5-phosphate.* BMC Microbiology, 2008. **8**(1): p. 98.

37. Nijhout, H.F., et al., *A mathematical model of the folate cycle: new insights into folate homeostasis.* J Biol Chem, 2004. **279**(53): p. 55008-16.

38. Kocsis, M.G., et al., *Insertional Inactivation of the Methionine S-Methyltransferase Gene Eliminates the S-Methylmethionine Cycle and Increases the Methylation Ratio.* Plant Physiol., 2003. **131**(4): p. 1808-1815.

39. Thomas, D., A. Becker, and Y. Surdin-Kerjan, *Reverse Methionine Biosynthesis fromS-Adenosylmethionine in Eukaryotic Cells.* Journal of Biological Chemistry, 2000. **275**(52): p. 40718-40724.

40. Gutierrez, J.A., et al., *Transition state analogs of 5'-methylthioadenosine nucleosidase disrupt quorum sensing.* Nat Chem Biol, 2009. **5**(4): p. 251-7.

41. Bebien, M., et al., *Involvement of Superoxide Dismutases in the Response of Escherichia coli to Selenium Oxides.* J. Bacteriol., 2002. **184**(6): p. 1556-1564.

42. Tagmount, A., A. Berken, and N. Terry, *An Essential Role of S-Adenosyl-L-Methionine:L-Methionine S-Methyltransferase in Selenium Volatilization by Plants. Methylation of Selenomethionine to Selenium-Methyl-L-Selenium- Methionine, the Precursor of Volatile Selenium.* Plant Physiol., 2002. **130**(2): p. 847-856.

43. Thanbichler, M., B. Neuhierl, and A. Bock, *S-Methylmethionine Metabolism in Escherichia coli.* J. Bacteriol., 1999. **181**(2): p. 662-665.

44. Bourgis, F., et al., *S-Methylmethionine Plays a Major Role in Phloem Sulfur Transport and Is Synthesized by a Novel Type of Methyltransferase.* Plant Cell, 1999. **11**(8): p. 1485-1498.

45. Vinci, C.R. and S.G. Clarke, *Recognition of Age-damaged (R,S)-Adenosyl-L-methionine by Two Methyltransferases in the Yeast Saccharomyces cerevisiae.* Journal of Biological Chemistry, 2007. **282**(12): p. 8604-8612.

46. Vinci, C.R. and S.G. Clarke, *Homocysteine Methyltransferases Mht1 and Sam4 Prevent the Accumulation of Age-damaged (R,S)-AdoMet in the Yeast Saccharomyces cerevisiae.* Journal of Biological Chemistry, 2010. **285**(27): p. 20526-20531.

47. Martinez-Gomez, N.C., M. Robers, and D.M. Downs, *Mutational analysis of ThiH, a member of the radical S-adenosylmethionine (AdoMet) protein superfamily.* J Biol Chem, 2004. **279**(39): p. 40505-10.

48. Ranocha, P., et al., *Characterization and functional expression of cDNAs encoding methionine-sensitive and -insensitive homocysteine S-methyltransferases from Arabidopsis.* J Biol Chem, 2000. **275**(21): p. 15962-8.

49. Ranocha, P., et al., *The S-methylmethionine cycle in angiosperms: ubiquity, antiquity and activity.* The Plant Journal, 2001. **25**(5): p. 575-584.

50. Roe, A.J., et al., *Inhibition of Escherichia coli growth by acetic acid: a problem with methionine biosynthesis and homocysteine toxicity.* Microbiology, 2002. **148**(Pt 7): p. 2215-22.

51. Jakubowski, H., *Proofreading in vivo: editing of homocysteine by methionyl-tRNA synthetase in Escherichia coli.* Proc Natl Acad Sci U S A, 1990. **87**(12): p. 4504-8.

52. Jakubowski, H., *Proofreading in vivo: editing of homocysteine by methionyl-tRNA synthetase in the yeast Saccharomyces cerevisiae.* Embo j, 1991. **10**(3): p. 593-8.

53. Christopher, S.A., et al., *S-Adenosylhomocysteine, but not homocysteine, is toxic to yeast lacking cystathionine β-synthase.* Molecular Genetics and Metabolism, 2002. **75**(4): p. 335-343.

54. Plamann, M.D. and G.V. Stauffer, *Regulation of the Escherichia coli glyA gene by the metR gene product and homocysteine.* J Bacteriol, 1989. **171**(9): p. 4958-62.

55. Byerly, K.A., M.L. Urbanowski, and G.V. Stauffer, *The metR binding site in the Salmonella typhimurium metH gene: DNA sequence constraints on activation.* Journal of Bacteriology, 1991. **173**(11): p. 3547-3553.

56. Urbanowski, M.L. and G.V. Stauffer, *Regulation of the metR gene of Salmonella typhimurium.* Journal of Bacteriology, 1987. **169**(12): p. 5841-5844.

57. Weissbach, H. and N. Brot, *Regulation of methionine synthesis in Escherichia coli.* Mol Microbiol, 1991. **5**(7): p. 1593-7.

58. Shoeman, R., et al., *Regulation of Methionine Synthesis in Escherichia coli: Effect of metJ Gene Product and S-adenosylmethionine on the Expression of the metF Gene.* Proceedings of the National Academy of Sciences of the United States of America, 1985. **82**(11): p. 3601-3605.

59. Shoeman, R., et al., *Regulation of methionine synthesis in Escherichia coli: Effect of metJ gene product and S-adenosylmethionine on the in vitro expression of the metB, metL and metJ genes.* Biochemical and Biophysical Research Communications, 1985. **133**(2): p. 731-739.

60. Kang, L., et al., *Upregulation of MetC Is Essential for d-Alanine-Independent Growth of an alr/dadX-Deficient Escherichia coli Strain.* Journal of Bacteriology, 2011. **193**(5): p. 1098-1106.

61. Maxon, M.E., et al., *Regulation of methionine synthesis in Escherichia coli: effect of the MetR protein on the expression of the metE and metR genes.* Proceedings of the National Academy of Sciences, 1989. **86**(1): p. 85-89.

62. !!! INVALID CITATION !!!

63. Cai, X.Y., et al., *Methionine synthesis in Escherichia coli: effect of the MetR protein on metE and metH expression.* Proceedings of the National Academy of Sciences, 1989. **86**(12): p. 4407-4411.

64. Cai, X.-Y., et al., *The effect of homocysteine on metR regulation of metE, metR and metH expression in vitro.* Biochemical and Biophysical Research Communications, 1989. **163**(1): p. 79-83.

65. Marincs, F., et al., *Transcript analysis reveals an extended regulon and the importance of protein–protein co-operativity for the Escherichia coli methionine repressor.* Biochem J, 2006. **396**(2): p. 227-234.

66. Fritsch, P.S., M.L. Urbanowski, and G.V. Stauffer, *Role of the RNA Polymerase α Subunits in MetR-Dependent Activation of metE and metH: Important Residues in the*

C-Terminal Domain and Orientation Requirements within RNA Polymerase. Journal of Bacteriology, 2000. **182**(19): p. 5539-5550.

67. Lorenz, E. and G.V. Stauffer, *Characterization of the MetR binding sites for the glyA gene of Escherichia coli.* J Bacteriol, 1995. **177**(14): p. 4113-20.

68. Wu, W.-F., M.L. Urbanowski, and G.V. Stauffer, *MetJ-mediated regulation of the Salmonella typhimurium metE and metR genes occurs through a common operator region.* FEMS Microbiology Letters, 1993. **108**(2): p. 145-150.

69. Urbanowski, M.L. and G.V. Stauffer, *Role of homocysteine in metR-mediated activation of the metE and metH genes in Salmonella typhimurium and Escherichia coli.* Journal of Bacteriology, 1989. **171**(6): p. 3277-3281.

70. Old, I.G., et al., *Regulation of methionine biosynthesis in the enterobacteriaceae.* Progress in Biophysics and Molecular Biology, 1991. **56**(3): p. 145-185.

71. Segel, I.H., *Biochemical calculations: how to solve mathematical problems in general biochemistry*. 1976: Wiley.

72. Matthews, R.G., *[58] Methylenetetrahydrofolate reductase from pig liver*, in *Methods in Enzymology*, D.B.M. Frank Chytil, Editor. 1986, Academic Press. p. 372-381.

73. Fu, T.F., et al., *Role of proline residues in the folding of serine hydroxymethyltransferase.* J Biol Chem, 2003. **278**(33): p. 31088-94.

74. Strader, M.B., et al., *Role of S65, Q67, I68, and Y69 Residues in Homotetrameric R67 Dihydrofolate Reductase†.* Biochemistry, 2001. **40**(38): p. 11344-11352.

75. Trimmer, E.E., et al., *Folate activation and catalysis in methylenetetrahydrofolate reductase from Escherichia coli: roles for aspartate 120 and glutamate 28.* Biochemistry, 2001. **40**(21): p. 6216-26.

76. Baccanari, D.P., et al., *Escherichia coli dihydrofolate reductase: isolation and characterization of two isozymes.* Biochemistry, 1977. **16**(16): p. 3566-3572.

77. Giladi, M., et al., *FolM, A New Chromosomally Encoded Dihydrofolate Reductase in Escherichia coli.* Journal of Bacteriology, 2003. **185**(23): p. 7015-7018.

78. Halliday, N.M., et al., *Quantitative liquid chromatography-tandem mass spectrometry profiling of activated methyl cycle metabolites involved in LuxS-dependent quorum sensing in Escherichia coli.* Analytical Biochemistry, 2010. **403**(1-2): p. 20-29.

79. Link, H., B. Anselment, and D. Weuster-Botz, *Leakage of adenylates during cold methanol/glycerol quenching of Escherichia coli.* Metabolomics, 2008. **4**(3): p. 240-247.

80. Hengge-Aronis, R., *Signal transduction and regulatory mechanisms involved in control of the sigma(S) (RpoS) subunit of RNA polymerase.* Microbiol Mol Biol Rev, 2002. **66**(3): p. 373-95, table of contents.

81. Tweeddale, H., L. Notley-McRobb, and T. Ferenci, *Effect of Slow Growth on Metabolism of Escherichia coli, as Revealed by Global Metabolite Pool ("Metabolome") Analysis.* Journal of Bacteriology, 1998. **180**(19): p. 5109-5116.

82. Simpson, E.H., *The interpretation of interaction in contingency tables.* Journal of the Royal Statistical Society. Series B (Methodological), 1951: p. 238-241.

83. Acharya, A.P., et al., *Metabolic engineering of lactate dehydrogenase rescues mice from acidosis.* Sci. Rep., 2014. **4**.

84. Phua, K.K.L., K.W. Leong, and S.K. Nair, *Transfection efficiency and transgene expression kinetics of mRNA delivered in naked and nanoparticle format.* Journal of Controlled Release, 2013. **166**(3): p. 227-233.

85. Lopes da Silva, F., et al., *Epilepsies as dynamical diseases of brain systems: basic models of the transition between normal and epileptic activity.* Epilepsia, 2003. **44 Suppl 12**: p. 72-83.

86. Joice, R. and M. Lipsitch, *Targeting Imperfect Vaccines against Drug-Resistance Determinants: A Strategy for Countering the Rise of Drug Resistance.* PLoS ONE, 2013. **8**(7): p. e68940.

87. Bonhoeffer, S., M. Lipsitch, and B.R. Levin, *Evaluating treatment protocols to prevent antibiotic resistance.* Proceedings of the National Academy of Sciences, 1997. **94**(22): p. 12106-12111.

Biography

Inderpreet, "Inder," Singh Jalli was born in Bombay, India in 1982. After graduating from high school, he completed a double-B.S. at University of Houston, Central Campus in 2005 in Biochemistry and Psychology with a minor in Chemistry. Inder is a member of the Sigma Xi Honor Society, and is a recipient of the Biology Grant-in-Aid for multiple years.